DESIGN OF BI-DIRECTIONAL CHARGER FOR SOLAR ELECTRIC VEHICLES

Thesis submitted in fulfillment of the requirements for the degree
of
MASTER OF TECHNOLOGY
in
Power System Engineering

Submitted By:
Aman Khokhar
Roll no. 2K20/PSY/02

Under the supervision of:
Dr. Alka Singh

DEPARTMENT OF ELECTRICAL ENGINEERING
DELHI TECHNOLOGICAL UNIVERSITY
(Formerly Delhi College of Engineering)
Bawana Road, Delhi - 110042

DEPARTMENT OF ELECTRICAL ENGINEERING

DELHI TECHNOLOGICAL UNIVERSITY
(Formerly Delhi College of Engineering)
Bawana Road, Delhi - 110042

CANDIDATE'S DECLARATION

I, Aman Khokhar, Roll No. 2k20/PSY/02 of M.Tech Power System engineering, hereby declare that the project dissertation titled "DESIGN OF BI-DIRECTIONAL CHARGER FOR SOLAR ELECTRIC VEHICLES" which is submitted by me to the Department of Electrical engineering, Delhi Technological University, Delhi in partial fulfillment of the requirement for the award of the degree of Master of Technology, is original and not copied from any source without proper citation. This work has not previously formed the basis for the award of any Degree, Diploma Associateship, Fellowship or other similar title or recognition.

Date:
Place:

Aman Khokhar

DEPARTMENT OF ELECTRICAL ENGINEERING

DELHI TECHNOLOGICAL UNIVERSITY
(Formerly Delhi College of Engineering)
Bawana Road, Delhi - 110042

CERTIFICATE

This is to certify that the thesis entitled, "**Design of Bi-Directional charger for Solar electric vehicles**" submitted by Aman Khokhar, Rollno: 2k20/PSY/02, Electrical engineering, Delhi Technological University in partial fulfillment of the requirements for the award of the degree of Master of Technology in Electrical Engineering at the Delhi Technological University is an authentic work carried out by him under my supervision and guidance. To the best of my knowledge, the matter embodied in the thesis has not been submitted to any other University/ Institute for the award of any degree or diploma.

Date:
Place:

Supervisor
Dr. Alka Singh
Department of Electrical Engineering
Delhi Technological University

Contents

List of Tables

List of Figures

List of Symbols, Abbreviation and Nomenclature

EV	Electric Vehicle
PV	Photovoltaic cell
PI	Proportional Integral
PD	Proportional Derivative
PID	Proportional Integral Derivative
PWM	Phase Width Modulation
V2G	Vehicle-to-Grid
G2V	Grid-to-Vehicle
PHEV	Photovoltaic Hybrid Electric Vehicle
PEV	Photovoltaic Electric Vehicle
AC	Alternating Current
DC	Direct Current
VDC	Voltage of Direct Current
ANN	Artificial Neural Network

ABSTRACT

Growing concerns about environmental issues are leading many countries to take steps that allow for rational use of energy and a sustainable future. Improving system efficiency and the use of renewable resources are some of the issues that need to be addressed in order to reduce emissions. That is why the flow of electricity is attracting the attention of companies, countries and research teams, as an important step in addressing the negative effects of current energy use. With the growing popularity of electric vehicle technology it is also important to address the charging and equipment requirements.

The combination of solar power and electric vehicle (EV) is key to greatly reducing our dependence on fossil fuels. Electricity comes from a variety of sources and it is important that electric vehicles are powered by renewable energy. Electric cars are becoming more popular and in the coming years we expect that almost anyone who owns a solar power system will install a solar charging station at home. Solar-powered electric cars in the interior building are also important for a sustainable future. Being able to transfer electricity from everyday cars or home systems to the grid can help support future energy needs.

This thesis focuses on the symbiotic relationship between individual solar systems and solar powered vehicles and the power grid. It proposes bi-directional charging system that could take energy from the grid to charge the vehicle as well as transfer excess power back to the grid to help out the electricity demands. If such a system is implemented on a large scale with every individual solar vehicle owner using their excess power generated in their vehicles to power the grid, then solar vehicles could become a major power source for the power grids. The proposed system is simulated in MATLAB Simulink and artificial intelligence is used to improve system performance of such a system. Both artificial neural network control and traditional control and then compared and plotted.

Chapter 1
Introduction

Electric Vehicles (EVs) currently make up a small percentage of vehicles sold around the world. But with growing concerns of global warming and depleting crude oil reserves resulting in increasing fuel prices have increased the demand for EVs. Many new vehicle buyers are considering EVs as their next purchase but many people have concerns about prices, charging and range of the vehicle. Fortunately, as EV technology is getting better everyday, the cost of EVs is dropping along with an increase in range and battery capacities, as well as lower maintenance cost. EVs are looking much more attractive to regular buyers, especially ones with rooftop solar. Being able to charge the vehicle through rooftop solar has increased the battery life and range of EVs significantly. Charging your own solar generated electricity can remove the fuel cost entirely. But that poses another challenge for EV owners.

The ability to charge EVs from solar as well as through the grid could help eliminate this problem. Being able to charge the EV from the grid along with the rooftop solar allows EV users a more sustainable way to power their vehicles in case of lack of sunlight or other factors which deter the working of rooftop solar. This also opens the possibility for EV users to transfer the excess energy back to the grid using bi-directional chargers, and by doing so grid owners or local governing bodies could offer ‘financial benefits or reduction in electricity bills’ as a return and hence creating a sustainable environment which benefits both the grid and EV users. Bi-directional charging can be implemented to create a symbiotic relationship between the EV owners and the grid.

Bi-directional charging uses complex power electronic circuits which could cause instabilities in the system and hence the grid. Hence, it is very crucial to address the instabilities to maintain grid performance and power quality. With increase in artificial intelligence technologies, it is possible to improve system performance without incurring high equipment and logistics costs. Artificial neural network based control systems can achieve system goals faster and more efficiently compared to traditional controllers like PI, PD or PID.

1.1 Introduction

With global warming on rise, it is important to find sustainable alternatives to generate electricity for current as well as future electricity demands. Solar energy offers an excellent renewable alternate source of energy. Hence, to utilize solar power to its highest potential and efficiency is also very crucial to not waste any resources. Moreover, with the increasing amount of greenhouse gasses in the environment due to vehicle pollution is also alarming. Electric vehicles with in-build solar module systems offer the best solution to both the problems. Electric vehicles can be used as a power source for the main grid if everyone with a solar vehicle with excess power start transferring power back into the grid or use their excess power to power their homes or offices. This would allow for a sustainable environment for current as well as future power needs.

1.1.1 Related Work

In order to provide the benefits of a green energy economy, renewable energy resources are available great interest in intelligent grid technology that includes efficient distributed production communication and control. [1] Another function has been introduced in the automotive technology to the grid that allows for a double flow of energy between the electric car battery and the power grid. This allows for high load shaving, load production, power control and performance improvement of the power system. Implementing car-to-grid technology requires a dedicated electric car battery charger, which allows for double-directional flow of power between the power grid and the electric car battery.

[2] developed a dual-powered battery charger for electric vehicles (EVs) for Grid-to-Vehicle (G2V), Vehicle-to-Grid (V2G), and Vehicle-to-Home (V2H) technology. During the G2V operating mode the batteries are charged from the power grid with the current sinusoidal power feature and power unit. During V2G operating mode the energy stored in batteries can be restored to the power grid which contributes to the performance of the power system. In V2H operating mode batteries stored in batteries can be used to supply home loads during power outages, or to provide loads in areas without connecting to the power grid.

There is study [3] & [4] on EMC and the impact of the charging process on the grid connection and power electronics. [5] various developments in technologies related to EVs, PHEVs and infrastructure, such as wiring harnesses, connectors, communication units and electric power converters. There is an increase in research in [6] AI technology and Neural network based controllers [7] in the power sector for power system performance and power quality.

1.1.2 Thesis Objective

The main objective of this thesis is to provide a stable and efficient system for bi-directional charging for solar electric vehicles so on large scale they could be used to power the grids of the future. This thesis proposes a bi-directional charging system for single phase as well as three phase grids. The key contributions of this thesis is design and implementation of bi-directional charging systems in single phase and three phase systems and design and modeling of artificial neural network based controllers to improve system performance.

1.1.3 Scope of Work

The proposed work is the conceptual model on the present and future requirements regarding meeting power demand using renewable sources of energy and promoting use of EVs for utilities advantage. This thesis provides a review of bi-directional charging systems for solar EVs to power the grid. The key contributions include proposed ideas for using excess solar energy from EVs, designing of bi-directional converters, modeling and designing of bi-directional charging systems and introducing artificial neural networks in control schemes to improve performance and system performance.

1.2 Bi-Directional Charger

A bi-directional charger is capable of charging and discharging energy from the EV. It can either pull the power from the grid and charge the vehicle or it can transfer power from the vehicle to the grid. Unlike standard EV chargers, which charge using AC power from the grid, bi-directional chargers are far more sophisticated and involve complex power electronics to manage the energy flow from grid to vehicle and vice versa. Bi-directional charger consists of converters that transform DC power from the vehicle battery to AC power and AC power from the grid to DC power.

EVs with bidirectional charging capability can be used to power a home, feed energy back into the electricity grid and even provide backup power in the event of a blackout or emergency.

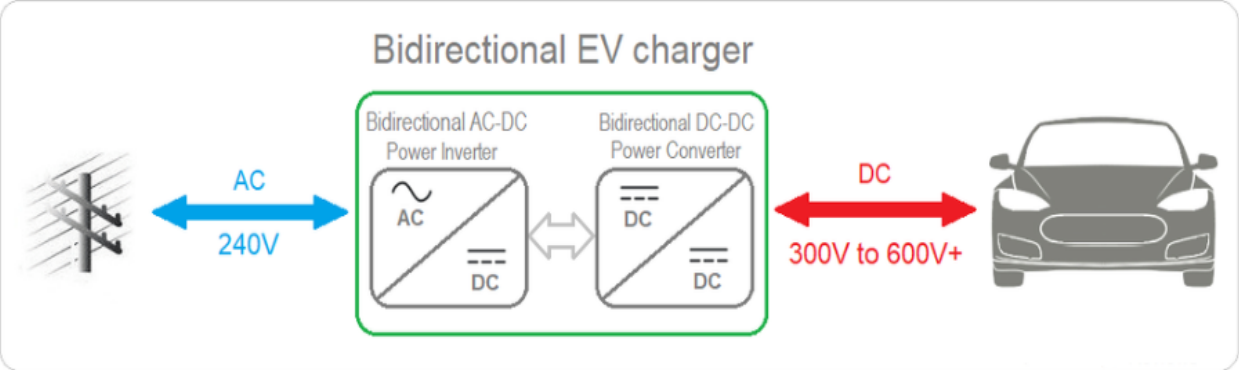

Figure 1.1: Schematic of Bi-directional EV charger

1.2.1 Types of Bi-Directional Charging

Bi-directional chargers can be used in various applications depending on needs and capabilities of the system:

- **Vehicle-to-grid (V2G):**
  Energy is exported from the battery to support the grid. This involves vehicles communicating with the power utilities and supplying power as needed. This can be a critical component for the power grid of the future. As it enables solar EVs to provide energy to the grid and could be a key source of power for the grid if multiple such vehicles are used together. It promotes the use of renewable sources of energy and reduces greenhouse gas emission.

- **Vehicle-to-Home (V2H):**
  A rooftop solar EV can provide power to a home or office and help out during power outages. Also households or offices could save money if they use EV's power source during the peak demand hours and charge the battery when electricity rates are lower.

- **Vehicle-to-Load (V2L)**
  Vehicle to load applications could have vehicles with in-build converters that could convert the DC voltage from battery to AC power so that vehicle could be plugged into loads.

- **Vehicle-to-Vehicle (V2V)**
  EVs have limited range on how far they could travel between charges. V2V charging allows one EV to charge another EV that is in need of charge. This could help overcome the range anxiety of EV users.

1.2.2 Circuit Diagram

Following is the circuit diagram for the bi-directional converter.

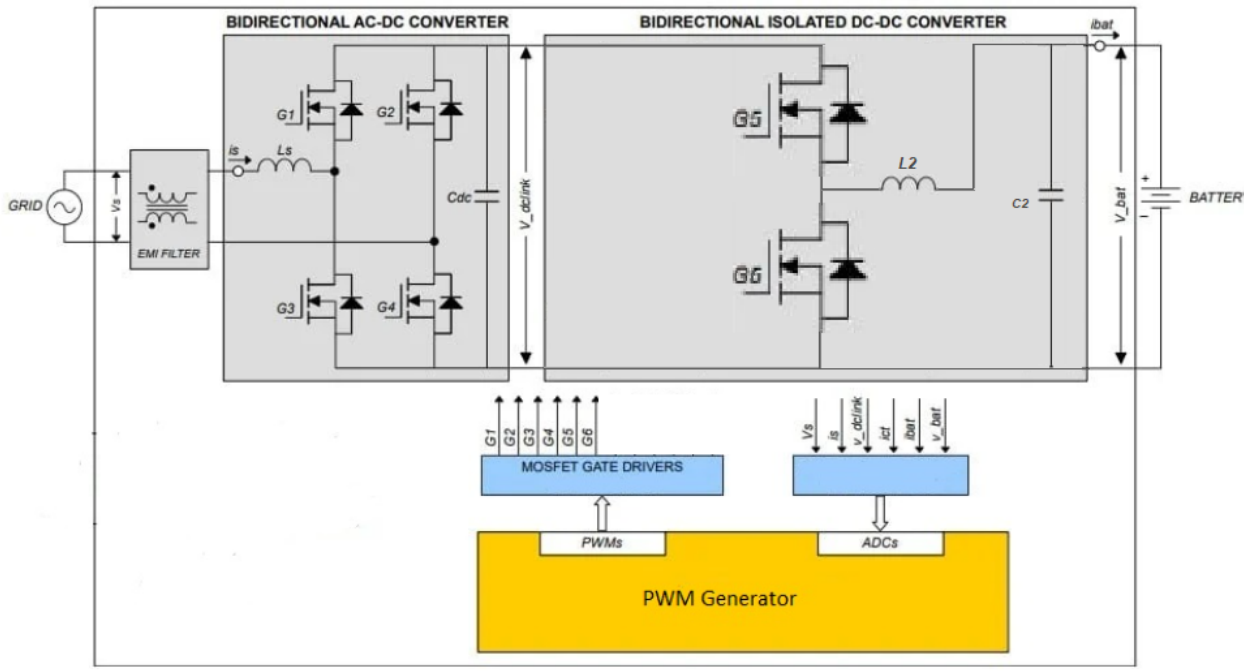

Figure 1.2: Bi-Directional Converter circuit diagram

This consists of an active rectifier (Bidirectional AC-DC converter) on the grid side which converts the AC voltage to DC and maintain constant voltage across the DC Bus and a Buck-Boost converter (Bidirectional isolated DC-DC converter) on the battery side used to control the battery current during charging and discharging operation. Both the converters are controlled using the waveforms from the PWM generator. [6]

1.3 Converter Design

In order to design each component for the converter, value of duty cycle, internal switch rating, input and output capacitance and inductance must be prepared. Following are the given parameters of the system for converter design based on the choice of microcontroller:

Table 1.1: System Parameters

Description	Parameter
Input voltage range	$V_{i(min)}$ to V_{IM}
Output voltage	V_o
Maximum output current	I_{OM}
Allowed current ripple	$I_{(L1)(pp)}$
Forward voltage drop of rectifier diode	V_f
Switching frequency	$f_{(SW)}$

1.3.1 Calculate Duty Cycle

First step is to calculate the steady state duty cycle for the inductive converters. This can be calculated from inductor and capacitor charge balance. For a robust design it is recommended to derive the duty cycle for the worst case scenario. For inverting buck-boost converters, it is maximum duty cycle (**D**) at minimum input voltage. Its is specified as:

$$D = \frac{-Vo + Vf}{-Vo + Vf + Vi(min)} \tag{1.1}$$

Rearranging Equation (2.1) provides the **DC conversion ratio V_o / V_i**

$$\frac{Vo}{Vi} = \frac{-D}{1-D} \tag{1.2}$$

1.3.2 Internal Switch (S1)

It is important to evaluate the rating for internal switch (S1) i.e. if it can withstand the output current. The minimum switching current limit ($\mathbf{I_{(SW)min}}$) of the internal switch (S1) must be higher or equal to the maximum switching current ($\mathbf{I_{(SW)M}}$) that is defined as:

$$I_{(SW)M} = I_{OM} \times \frac{V_{I(min)} + V_f - V_o}{V_{I(min)}} + \frac{I_{(L1)(pp)}}{2} \quad (1.3)$$

Maximum output current $\mathbf{I_{OM}}$ that converter can achieve can be calculated by rearranging (2.3) as:

$$I_{OM} = \left(\frac{V_{I(min)}}{V_{I(min)} + V_f - V_o}\right)\left(I_{(SW)min} + \frac{I_{(L1)(pp)}}{2}\right) \quad (1.4)$$

The maximum voltage the switch (S1) can withstand is $\mathbf{V_{(SW)M}}$ and can be derived as:

$$V_{(SW)M} = V_{IM} + V_f + V_o \quad (1.5)$$

1.3.3 Selecting the Inductor

The required value of the inductance ($\mathbf{L_1}$) can be estimated using:

$$L_1 = \frac{V_I D}{I_{(L1)(pp)} f_{SW}} \quad (1.6)$$

The average inductor current $\mathbf{I_{(L1)avg}}$ is calculated by:

$$I_{(L1)avg} = \frac{I_O}{1 - D} \quad (1.7)$$

1.3.4 Selecting the Capacitor

The input and output currents are pulsed in this converter. The choice of input and output capacitance values is very important to ensure system performance [7]. When choosing capacitance, DC Bias effect should be taken into account as capacitance of ceramic capacitors decreases with applied voltage. It's also recommended to choose capacitors with Equivalent Series Resistance (ESR) to be low (<10 mΩ) as higher value of equivalent series resistance of the capacitor (ESR) increases the input voltage drop.

(a) Input Capacitor

The input capacitor is required to store the input voltage during discharging of the inductor. If the input voltage drop shall not be bigger than $\mathbf{V_{I\,(pp)}}$, the minimum effective value for the capacitor $\mathbf{C_{I\,(min)}}$ can be estimated with:

$$C_{I\,(min)} = \frac{I_{(L1)avg} \times D}{f_{SW} \times [\,V_{I(pp)} - (I_{(L1)(pp)} \times ESR_{C1})]} \tag{1.9}$$

(b) Output Capacitor

The output current is discontinuous so the output capacitor is required to supply power to load during charging of the inductor. The output voltage ripple $\mathbf{V_{O\,(pp)}}$ can be estimated by:

$$V_{O(pp)} = \frac{I_O D}{f_{SW} C_O} + \left(\frac{I_O}{1-D} + \frac{I_{(L1)(pp)}}{2}\right) \times ESR_{CO} \tag{1.10}$$

The minimum required capacitance $\mathbf{C_{O\,(min)}}$ at an output voltage ripple requirement of $V_{O(pp)}$ given by:

$$C_{O(min)} = \frac{I_O D}{f_{SW} \times [\,V_{O(pp)} - (\frac{I_O}{1-D} + \frac{I_{(L1)(pp)}}{2}) \times ESR_{CO}]} \tag{1.11}$$

1.3.5 Calculation for given system

Battery and given system parameters are in the following table:

Table 2.2: Given System Parameters

Description	Parameter
Nominal Input voltage range	V_I = 160V
Output voltage	V_O = -230V
Forward voltage drop of rectifier diode	V_f = 0.7V
Allowed inductor current ripple	10μH
Equivalent Series Resistor (ESR)	5mΩ
Switching frequency	10KHz

Table 2.3: Calculated Converter Design Parameters

Description	Parameter
Maximum Duty Cycle (D)	$D = \frac{-(-230) + 0.7}{-(-230) + 0.7 + 150} = 0.60$
DC Conversion Ratio (V_o/V_I)	$\frac{Vo}{Vi} = \frac{-0.6}{1-0.6} = -1.5$
Maximum Output Current	$I_{OM} = (\frac{150}{150 + 0.7 - (-230)})(65 + \frac{12}{2}) = 27.6\text{A}$
Inductance (L_1)	$L_1 = \frac{V_I D}{I_{(L1)(pp)} f_{SW}} = \frac{160*0.6}{4.8\times10^3} = 20mH$
Minimum Input Capacitance ($C_{I(min)}$)	$C_{I\,(min)} = \frac{I_{(L1)avg} \times 0.6}{10^3 \times [\,(-160) - (4.8 \times 5\times10^{-3})]} = 5600\mu\text{F}$

1.4 Photovoltaic Module (PV)

The PV module [9] used for simulations have following specifications:

Table 3.1: Photovoltaic module parameters

Description	Parameter
Module	1 Soltech 1STH-215-P
Rated Power	215W
Cells per module (N_{cells})	60
Voltage at maximum power point (V_{MP})	29V
Current at maximum power point (I_{MP})	7.35A
Total number parallel strings	1
Series connected modules per string	10
Temperature coefficient of V_{OC}	-0.36(% / deg.C)

The PV module's power output changes along with the irradiance and temperature of the module. The simulations are done at constant temperature and irradiance.

Table 3.2: Temperature and irradiance of PV module for simulations

Description	Parameter
Irradiance	1000 W/m^2
Temperature	25 deg.C

Following is the plot for power (W) and current (A) vs voltage (V) for different irradiance values i.e. [1000 W/m^2 , 500 W/m^2 , 100 W/m^2]. Maximum power point (MPPT) is marked for each irradiance value.

.

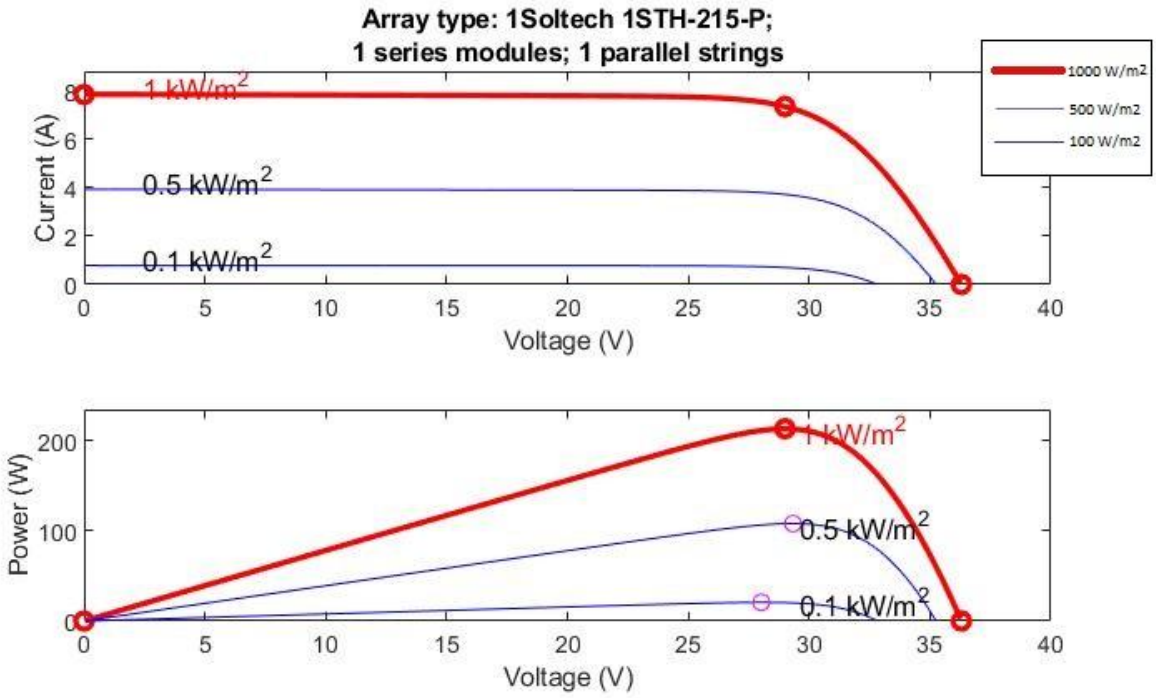

Figure 1.3: Power(W) and Current(A) vs Voltage(V) plot for different irradiance values

From the above plot we can observe that power output of PV modules is a function of temperature and irradiance. Hence, for the simulations temperature and irradiance are kept constant for initial simulations.

1.5 Electric Vehicle (EV)

EV is represented by a Lithium ion battery in all the simulations. Following are the parameters of the battery:

Table 3.3: Electric vehicle battery parameters

Description	Parameter
Nominal Voltage	160V
Rated Capacity	120 Ah
Full charge voltage	186V

Capacity at Nominal voltage	108.5V
Initial state of the charge	50%

Discharge characteristics of the battery[15] is given by following plot:

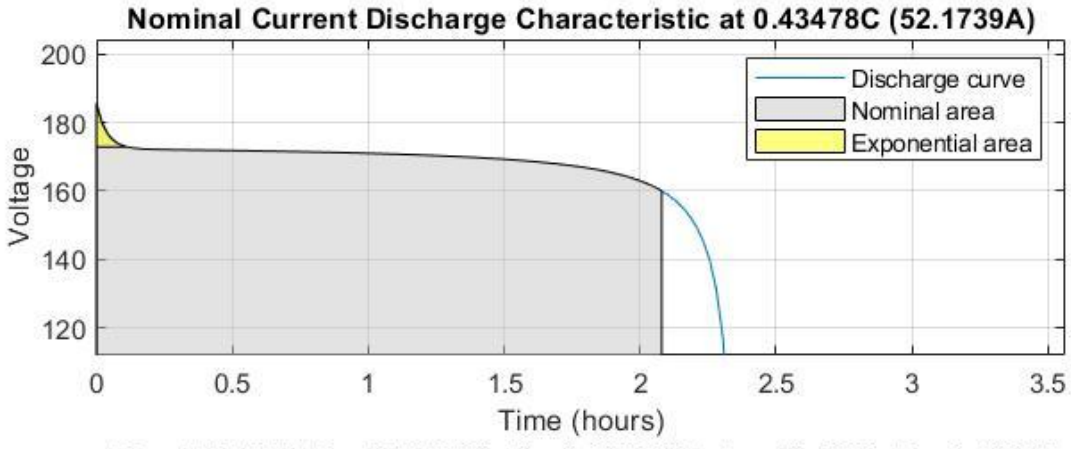

Figure 1.4: Battery discharge characteristics

1.6 Conclusion

For bi-directional converter design:

Nominal Input voltage range = 160V
Output voltage = -230V
Forward voltage drop of rectifier diode = 0.7V
Allowed inductor current ripple = 10μH
Equivalent Series Resistor (ESR) = 5mΩ
Switching frequency = 10KHz

Maximum Duty Cycle (D) = 0.60
DC Conversion Ratio (Vo/VI) = -1.5
Maximum Output Current = 27.6A
Inductance (L1) = 20mH
Minimum Input Capacitance (CI(min)) = 5600μF

Specifications of PV array

Module = 1 Soltech 1STH-215-P
Rated Power = 215W
Cells per module (Ncells) = 60
Voltage at maximum power point (VMP) = 29V
Current at maximum power point (IMP) = 7.35A
Total number parallel strings = 1
Series connected modules per string = 10
Temperature coefficient of VOC = -0.36(% / deg.C)

Electric Vehicle battery specifications

Nominal Voltage = 160V
Rated Capacity = 120 Ah
Full charge voltage = 186V
Capacity at Nominal voltage = 108.5V
Initial state of the charge = 50%

Chapter 2
Single Phase Operation

Bi-directional charging system can be used for single phase grids. EMI Filters, or electromagnetic interference filters, also called RFI Filters or radio-frequency interference filters, are used to mitigate the high frequency electromagnetic noise present on the power and signal lines. AC-DC converter is implemented on grid side after filtering for electromagnetic noise. High-volume capacitance [16] is required to buffer the power difference between the input and output ports in single phase grid-connected photovoltaic inverters, which become an obstacle to high system efficiency and long system's lifetime. [17] presented methods, which addressed the existing dc-link double-line-frequency voltage ripples in single-phase grid-connected PV inverters. DC-DC buck boost converter is used on the vehicle side to change DC voltage from solar PV or from the grid.

Following block diagram gives an overview of system configuration.

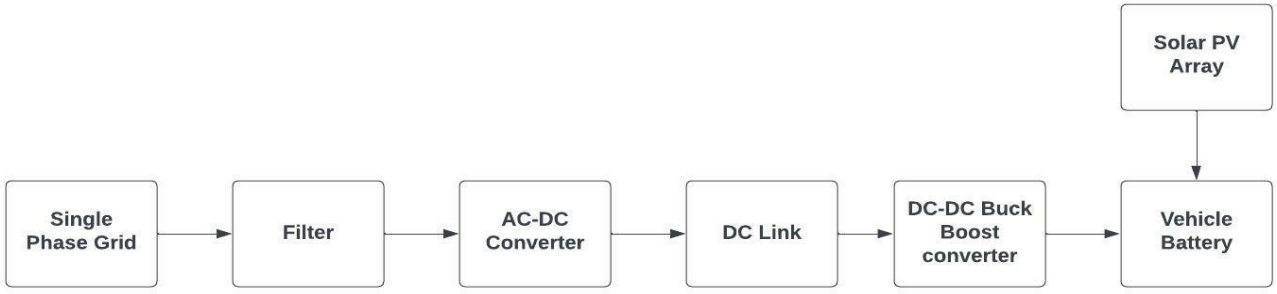

Figure 2.1: Single Phase Operation block diagram

2.1 Control Scheme

The control scheme for single phase operation consists of two parts. First is the PWM generation for gate control of AC-DC converter and second is for PWM generation for gate control of DC-DC buck boost converter. To synchronize the photovoltaic system output and the AC grid a PLL (phase-locked loop) was implemented, carrying out the angle detection in the grid. PID

controllers are used for error detection and correction and the final signal is fed to the PWM generator.

Following is the basic block diagram overview for AC-DC converter control:

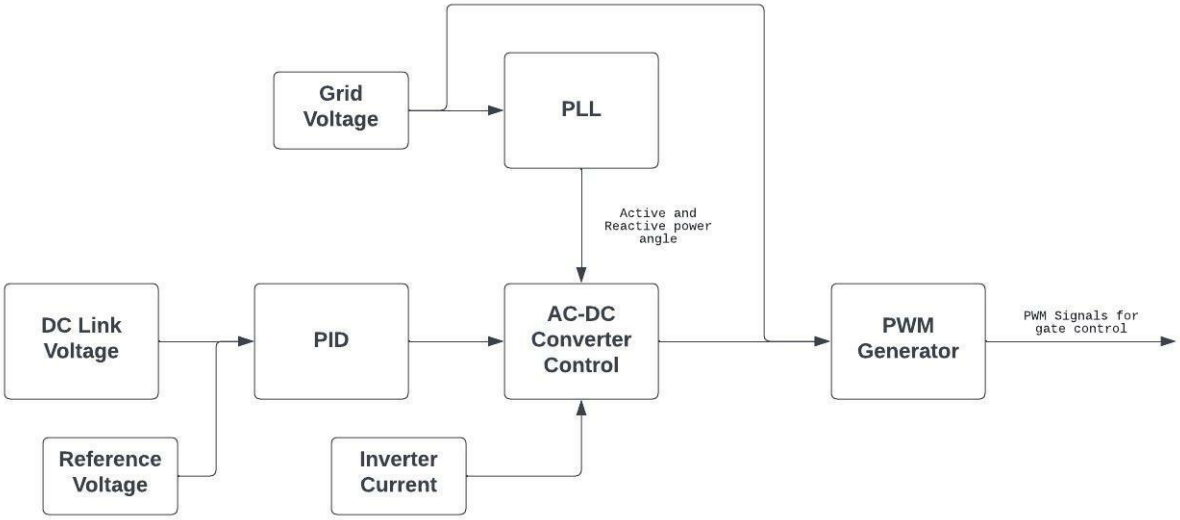

Figure 2.2: Basic block diagram for AC-DC converter control

The controller takes inputs as VDC which is compared against a reference voltage using a PI controller. Then the power angle of active component of power is multiplied giving :

$$e(t) = (V_{dc} - V_{ref}) \tag{2.1}$$

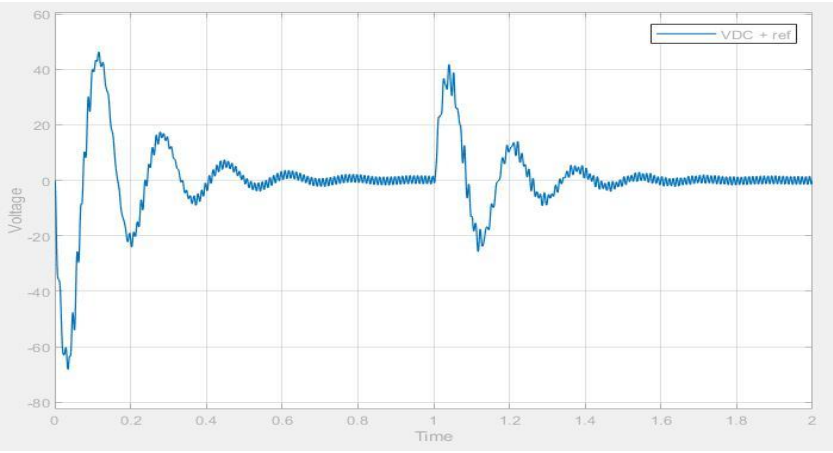

Figure 2.3: Plot of *Vdc + Vref*

$$C(t) = K_p e(t) + K_i \int e(t)dt \quad (2.2)$$

$$C(t) = 0.18e(t) + 20 \int e(t)dt \quad (2.3)$$

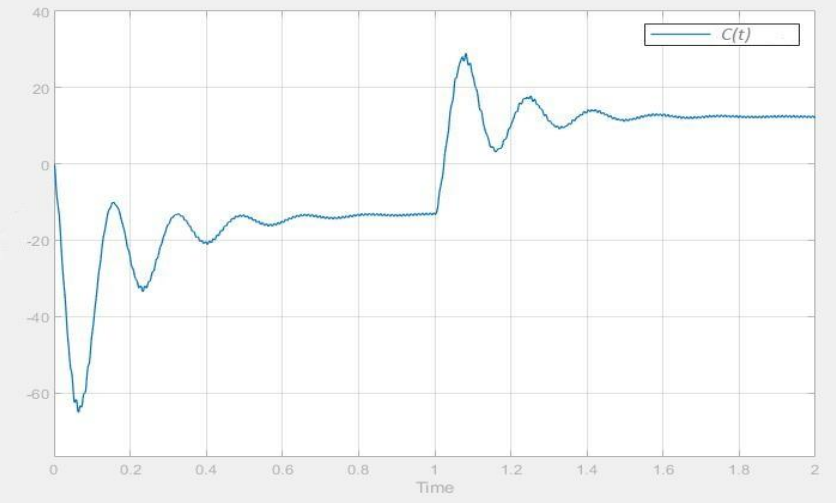

Figure 2.4: Plot of PID output: *C(t)*

Following is the plot of *C(t)sinθ* i.e. PID output multiplied by active power component angle

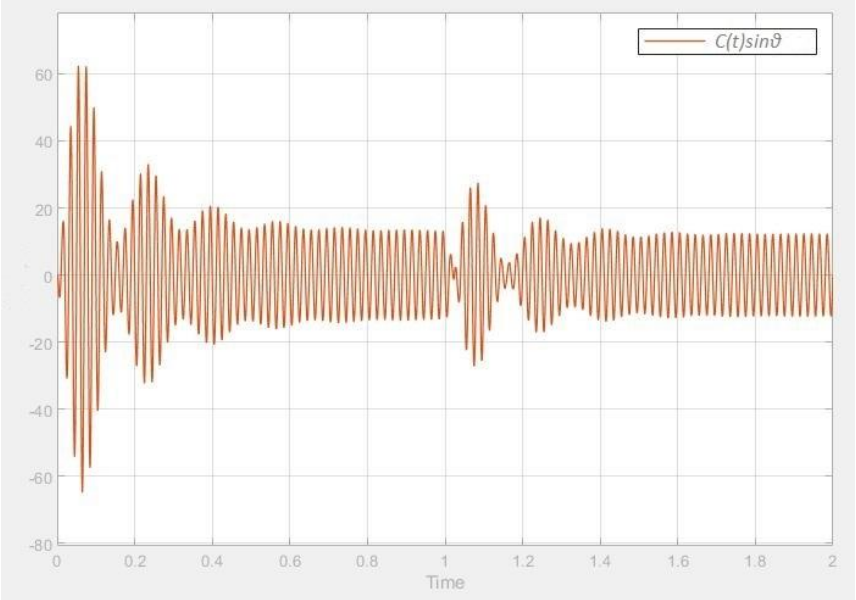

Figure 2.5: Plot of *C(t)sinθ*

$$A(t) = C(t)sin\theta - I_{inv} \quad (2.4)$$

$$B(t) = 10A(t) + 100A(t)\int A(t)dt - 200\pi f\frac{dA(t)}{dt} \quad (2.5)$$

And finally B(t) is added with grid voltage and fed to the PWM generator:

$$U(t) = B(t) + V_{GRID} \quad (2.6)$$

PWM generator for AC-DC converter is plotted in following graph:

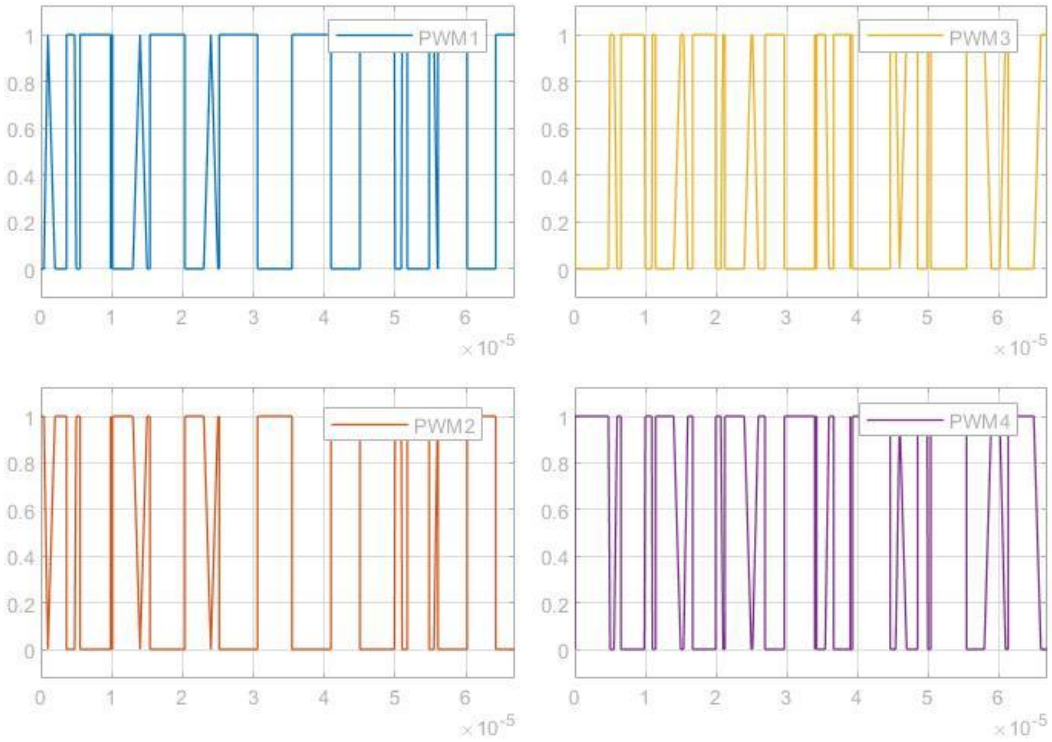

Figure 2.6: AC-DC converter PWM output

Following is the complete block diagram for AC-DC converter control system:

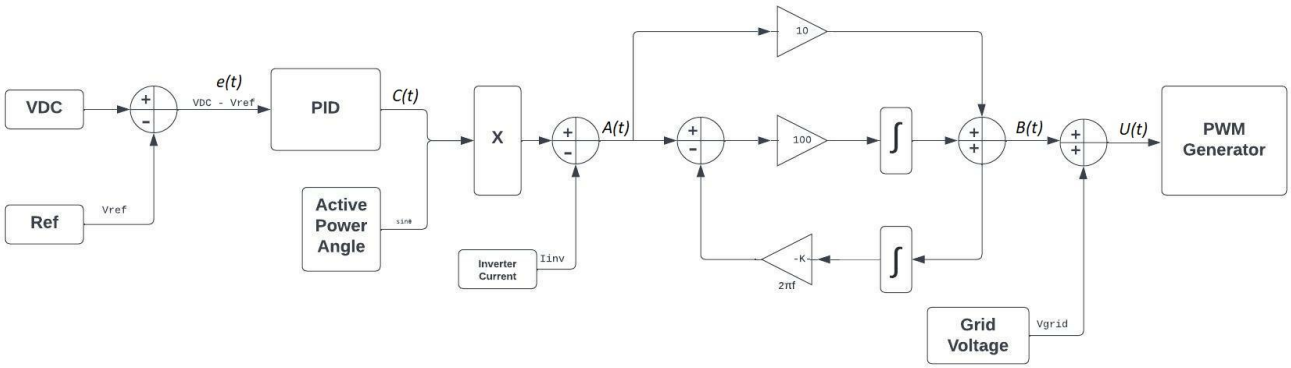

Figure 2.7: Control diagram for AC-DC converter

For DC-DC Buck Boost converter control, Battery current is compared with a reference current and error is calculated using a PI controller and output signal is fed to a PWM generator. PWM output is used for Buck mode and inverted for Boost mode.

$$r(t) = (I_{bat} - I_{ref}) \tag{2.1}$$

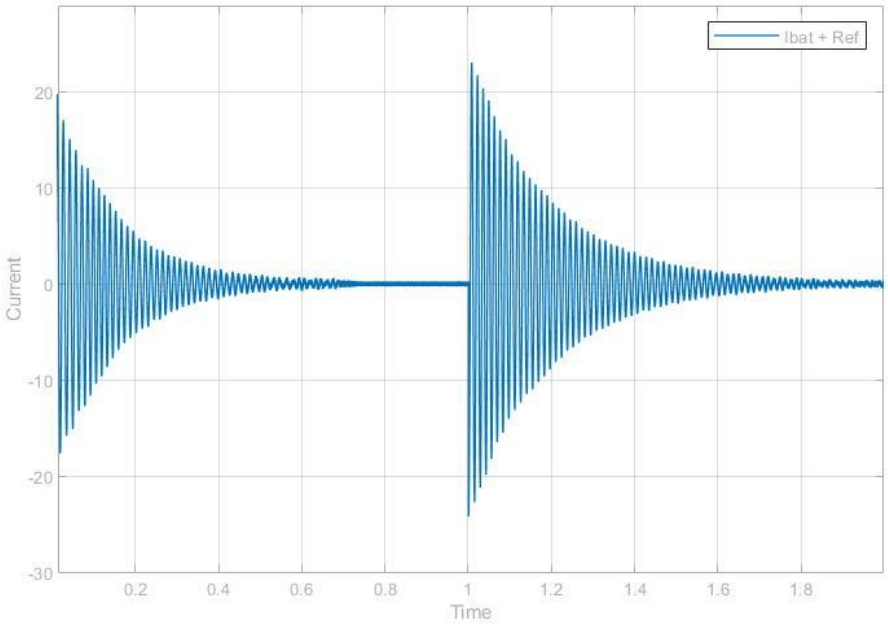

Figure 2.8: Plot of sum of battery current and reference current

$$U(t) = K_p r(t) + K_i \int r(t)dt \quad (2.2)$$

$$U(t) = 0.0005r(t) + 10 \int r(t)dt \quad (2.3)$$

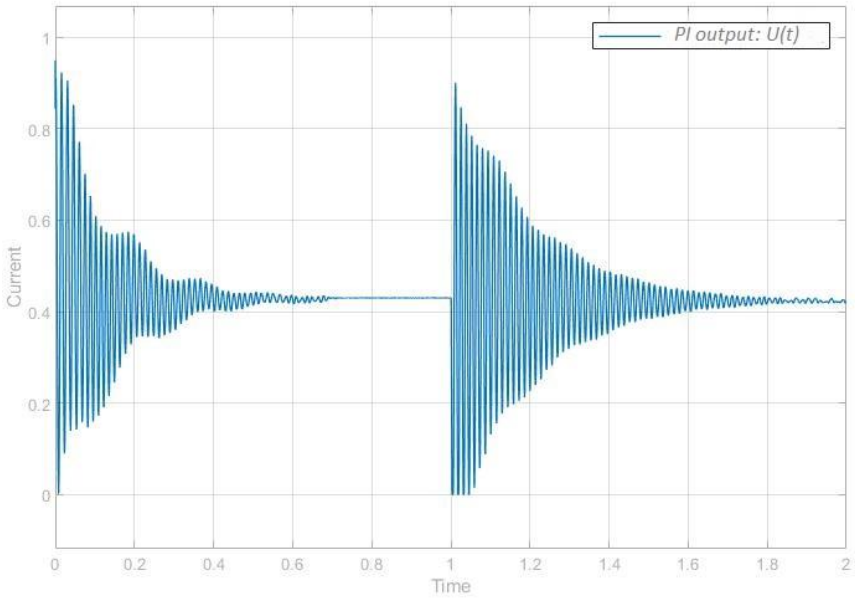

Figure 2.9: Plot of PI output: *U(t)*

Following is the complete control diagram for DC-DC buck boost converter:

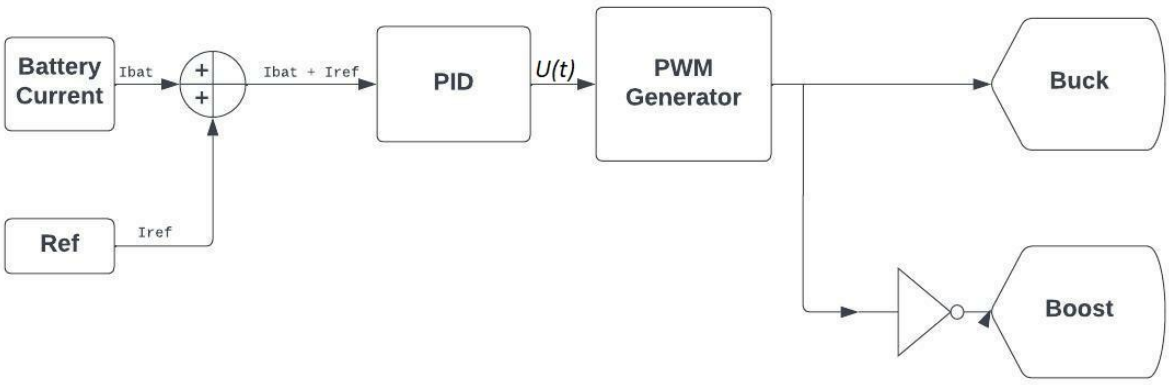

Figure 2.10: Control diagram for DC-DC Buck Boost converter

2.2 Simulation

Single phase operation of EV with PV modules in Vehicle-to-Grid (V2G) and Grid-to-Vehicle (G2V) modes is demonstrated in the simulation. Battery reference current can be changed to switch between the modes. Grid is connected to the EV battery via a bi-directional charging circuit.

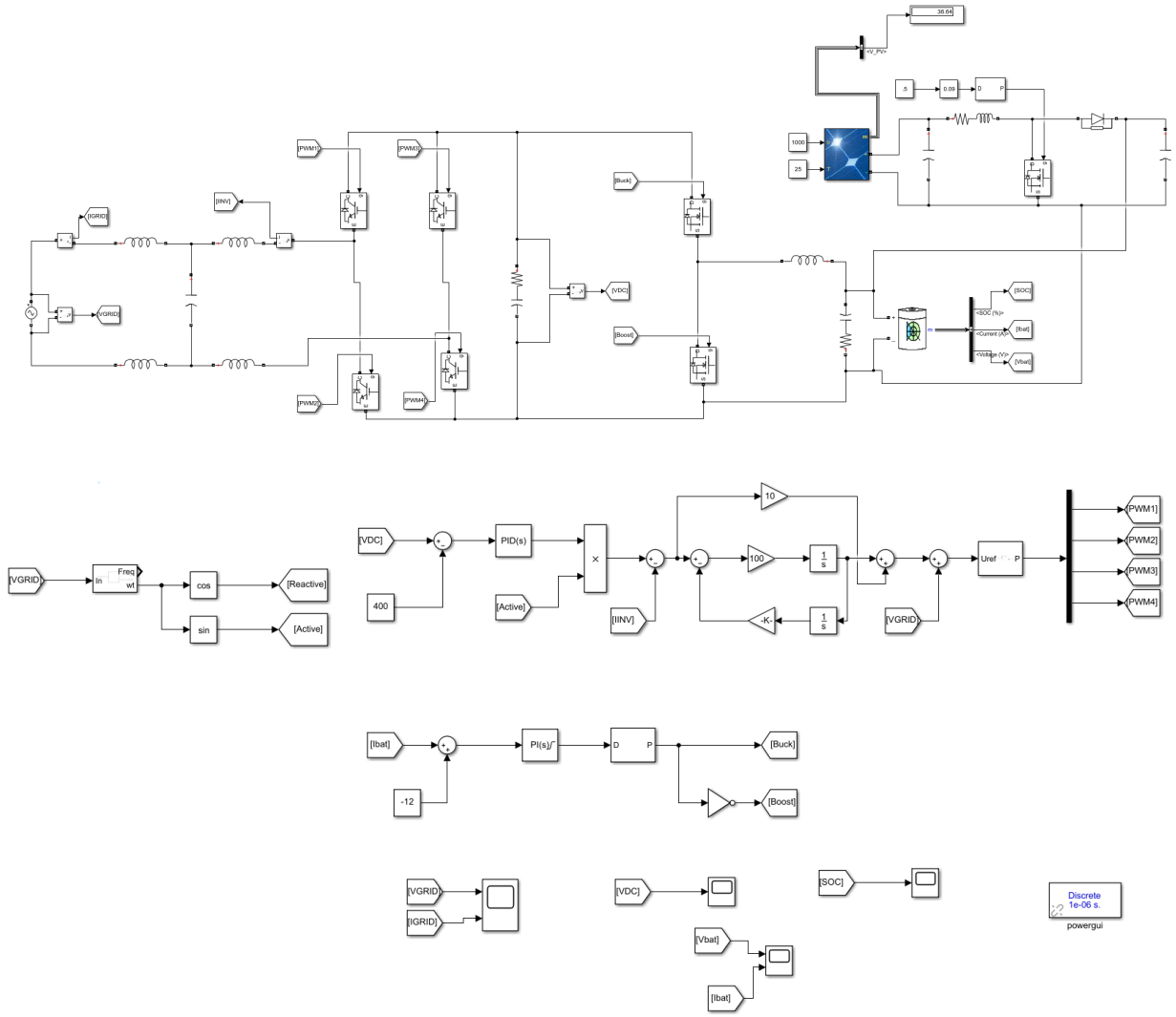

Figure 2.11: Single phase V2G and G2V MATLAB Simulink simulation

The simulation is in G2V mode and then switches to V2G mode at 1s. Power transfer from grid to battery and vice versa can be observed by grid voltage and grid current being in and out of phase respectively.

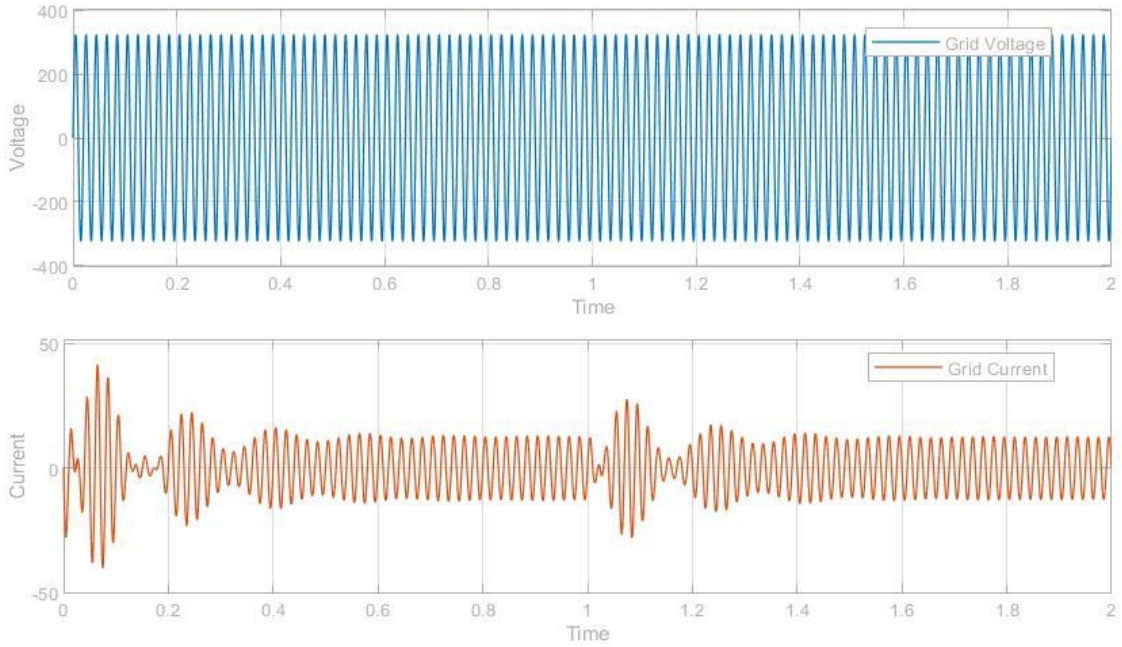

Figure 2.12: Grid voltage and Grid current

The system is in G2V mode. Hence, grid voltage and current are in phase with each other implying power transfer from grid to the battery.

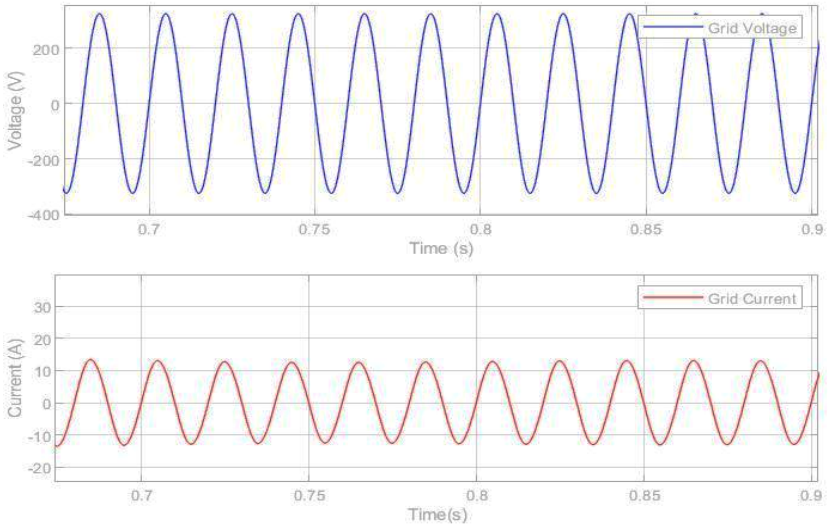

Figure 2.13: Grid voltage and current during G2V operation

The system is in V2G mode. Hence, grid voltage and current are out of phase with each other implying power transfer from battery to the grid.

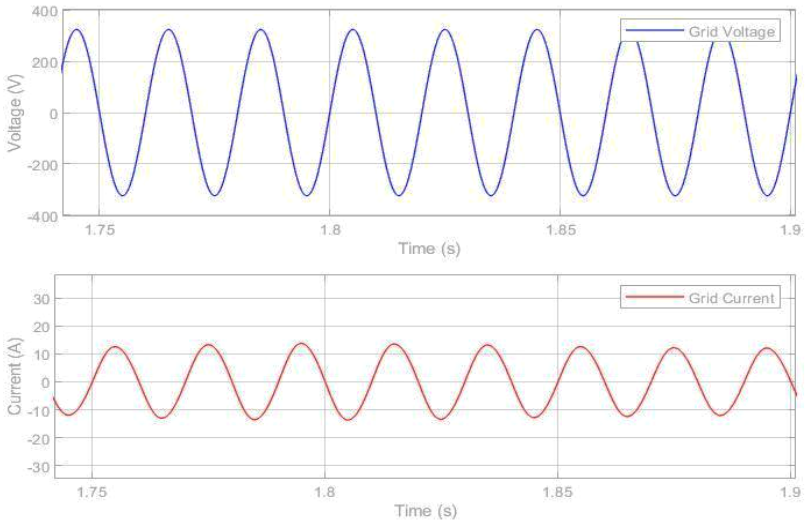

Figure 2.14: Grid voltage and current during G2V operation

State of charge (SOC) is the current level of charge relative to its capacity. SOC increases when the system is in G2V mode since power is transferred to the battery and decreases during V2G mode as battery is transferring power to the grid.

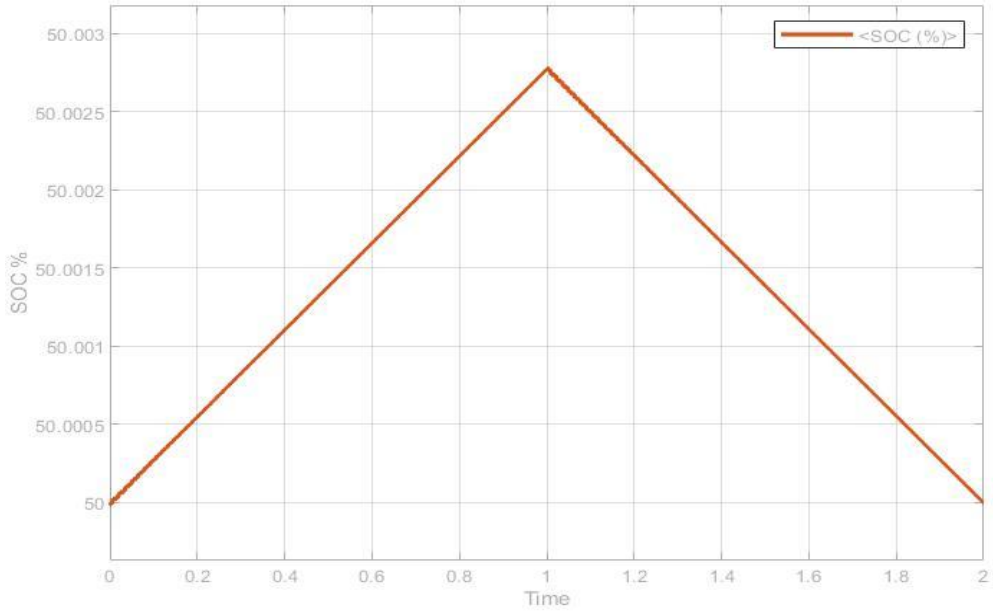

Figure 2.15: SOC % of the battery in single phase operation

VDC across the converter of bi-directional during simulation switching from G2V mode to V2G mode.

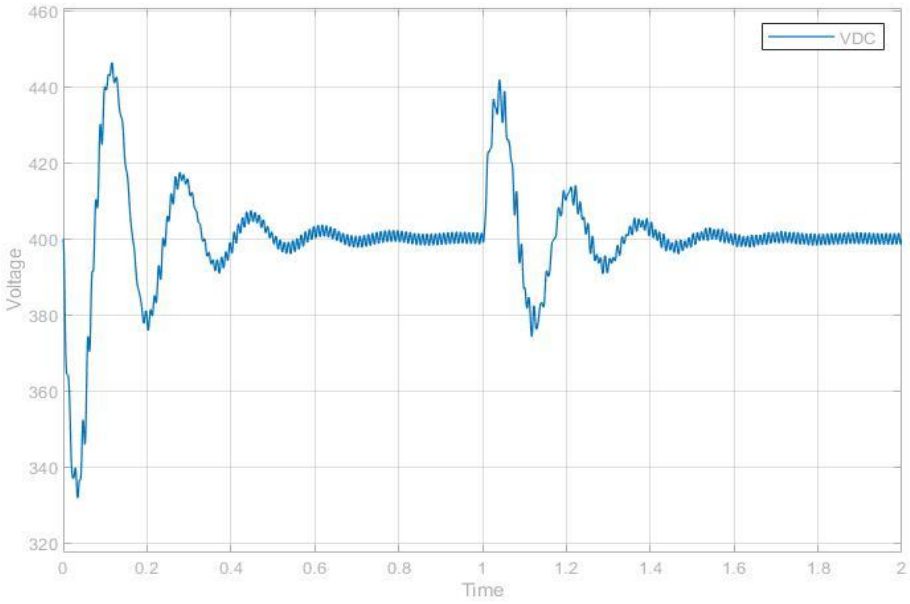

Figure 2.16: VDC during simulation

Battery current and battery voltage is represented by the following plot. The battery voltage increases during G2V and battery current is negative. The battery voltage decreases during V2G and battery current is positive.

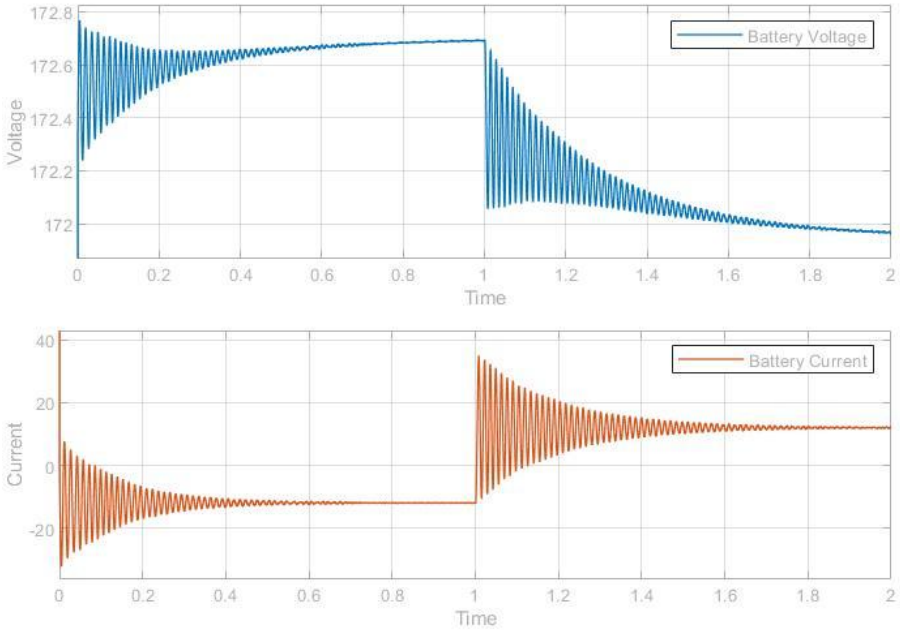

Figure 2.17: Battery current and Battery voltage

2.3 Conclusion

Single phase b-directional converter for solar EV is designed for both G2V and V2G operations and following parameter have observed:

EV Battery steady state current during G2V mode = -16.2 A
EV Battery steady state current during V2G mode = 16.3 A

EV Battery steady state voltage during G2V mode = 172.64 V
EV Battery steady state voltage during V2V mode = 171.93 V

Steady state VDC voltage ripple = 5V

% SOC increase after 1s of operation in G2V mode = 0.0027%

Chapter 3
Three Phase Operation

The system can be used for three phase operation with a 3-phase grid. The 3-phase grid is connected to the bi-directional converter using an EMI filter (Electromagnetic Interference filter), to mitigate the high frequency electromagnetic noise present in the 3-phase power line. EMI filter is connected with the AC-DC converter which converts the 415V 3-phase AC voltage into DC voltage. The DC link is connected with a DC-DC buck boost converter to change the power from the grid or from the EV battery. The EV battery is connected to a rooftop solar array through a DC-DC buck converter.

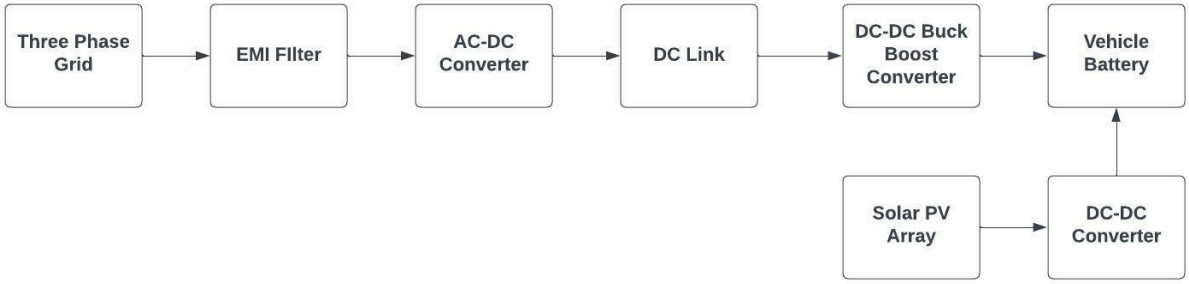

Figure 3.1: Overview of three phase operation

3.1 Clark and Park transforms

Clarke and Park transforms[18] are commonly used in field-oriented control of three-phase AC machines. The Clarke transform converts the time domain components of a three-phase system (in abc frame) to two components in an orthogonal stationary frame (αβ). The Park transform converts the two components in the αβ frame to an orthogonal rotating reference frame (dq).

Table 3.1: Clark and Park transformations

	Standard (Amplitude-Invariant)	Power-Invariant
Clarke abc to $\alpha\beta 0$	$\frac{2}{3}\begin{bmatrix} 1 & -\frac{1}{2} & -\frac{1}{2} \\ 0 & \frac{\sqrt{3}}{2} & -\frac{\sqrt{3}}{2} \\ \frac{1}{2} & \frac{1}{2} & \frac{1}{2} \end{bmatrix}$	$\sqrt{\frac{2}{3}}\begin{bmatrix} 1 & -\frac{1}{2} & -\frac{1}{2} \\ 0 & \frac{\sqrt{3}}{2} & -\frac{\sqrt{3}}{2} \\ \frac{1}{\sqrt{2}} & \frac{1}{\sqrt{2}} & \frac{1}{\sqrt{2}} \end{bmatrix}$

Park abc to $dq0$	$\frac{2}{3}\begin{bmatrix} \cos(\theta) & \cos(\theta-\frac{2\pi}{3}) & \cos(\theta+\frac{2\pi}{3}) \\ -\sin(\theta) & -\sin(\theta-\frac{2\pi}{3}) & -\sin(\theta+\frac{2\pi}{3}) \\ \frac{1}{2} & \frac{1}{2} & \frac{1}{2} \end{bmatrix}$	$\sqrt{\frac{2}{3}}\begin{bmatrix} \cos(\theta) & \cos(\theta-\frac{2\pi}{3}) & \cos(\theta+\frac{2\pi}{3}) \\ -\sin(\theta) & -\sin(\theta-\frac{2\pi}{3}) & -\sin(\theta+\frac{2\pi}{3}) \\ \frac{1}{\sqrt{2}} & \frac{1}{\sqrt{2}} & \frac{1}{\sqrt{2}} \end{bmatrix}$
Inverse Clarke $\alpha\beta 0$ to abc	$\begin{bmatrix} 1 & 0 & 1 \\ -\frac{1}{2} & \frac{\sqrt{3}}{2} & 1 \\ -\frac{1}{2} & -\frac{\sqrt{3}}{2} & 1 \end{bmatrix}$	$\sqrt{\frac{2}{3}}\begin{bmatrix} 1 & 0 & \frac{1}{\sqrt{2}} \\ -\frac{1}{2} & \frac{\sqrt{3}}{2} & \frac{1}{\sqrt{2}} \\ -\frac{1}{2} & -\frac{\sqrt{3}}{2} & \frac{1}{\sqrt{2}} \end{bmatrix}$
Inverse Park $dq0$ to abc	$\begin{bmatrix} \cos(\theta) & -\sin(\theta) & 1 \\ \cos(\theta-\frac{2\pi}{3}) & -\sin(\theta-\frac{2\pi}{3}) & 1 \\ \cos(\theta+\frac{2\pi}{3}) & -\sin(\theta+\frac{2\pi}{3}) & 1 \end{bmatrix}$	$\sqrt{\frac{2}{3}}\begin{bmatrix} \cos(\theta) & -\sin(\theta) & \frac{1}{\sqrt{2}} \\ \cos(\theta-\frac{2\pi}{3}) & -\sin(\theta-\frac{2\pi}{3}) & \frac{1}{\sqrt{2}} \\ \cos(\theta+\frac{2\pi}{3}) & -\sin(\theta+\frac{2\pi}{3}) & \frac{1}{\sqrt{2}} \end{bmatrix}$

V_{abc} of the 3-phase 415V grid is given by following graph:

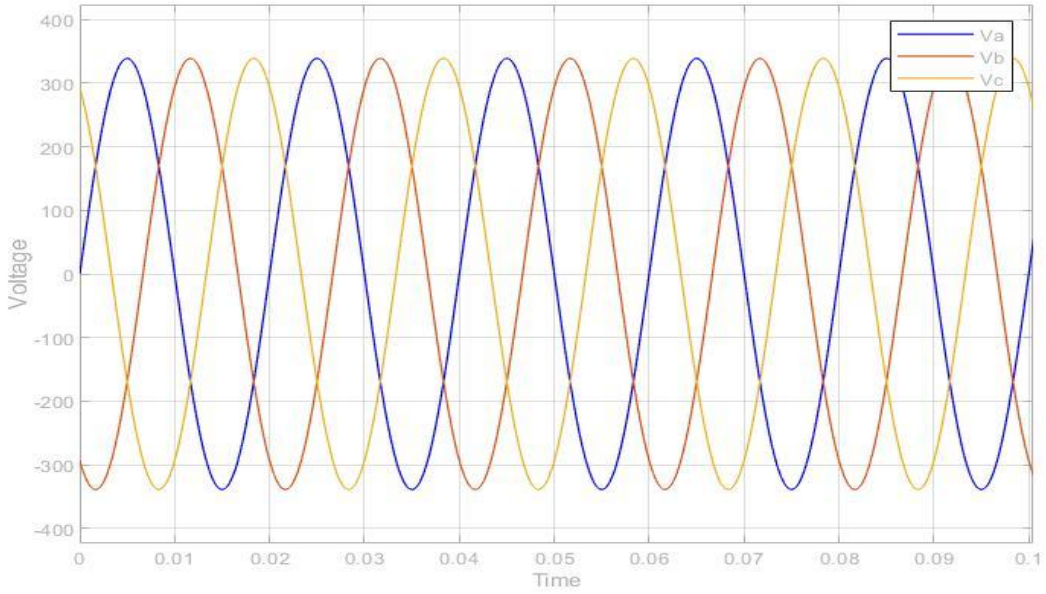

Figure 3.2: V_{abc} of the 3-phase 415V grid

Alpha-beta zero transform can be used in phase-locked loop (PLL) for synchronization purposes. 3-phase Grid V_{abc} is converted to alpha and beta using Clark transforms which is given as:

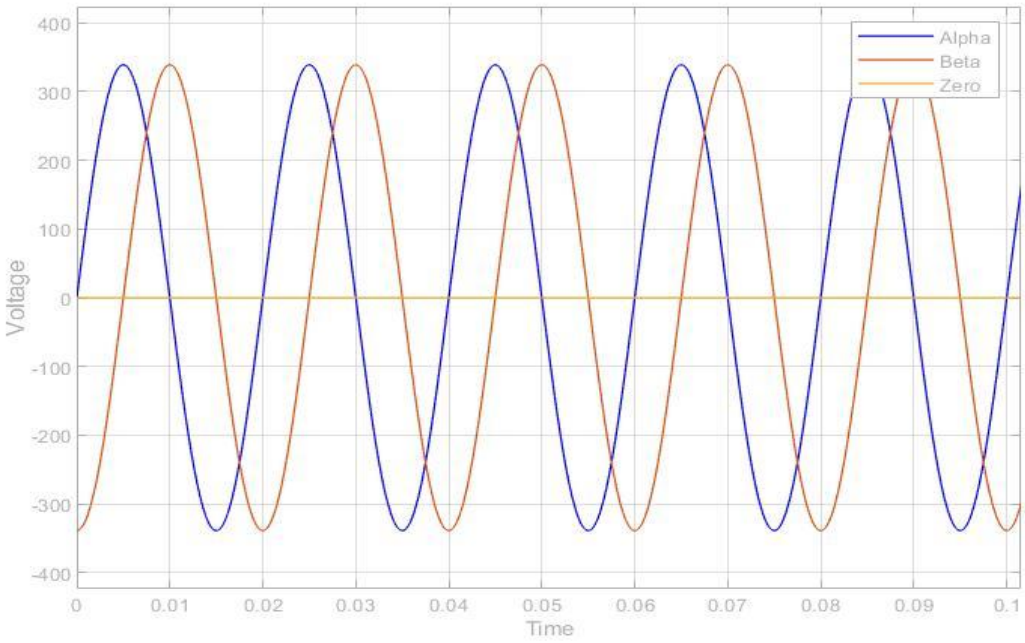

Figure 3.3: alpha-beta transform of Grid V_{abc}

3-phase Grid V_{abc} is converted to dq0 using Park transforms which is given as:

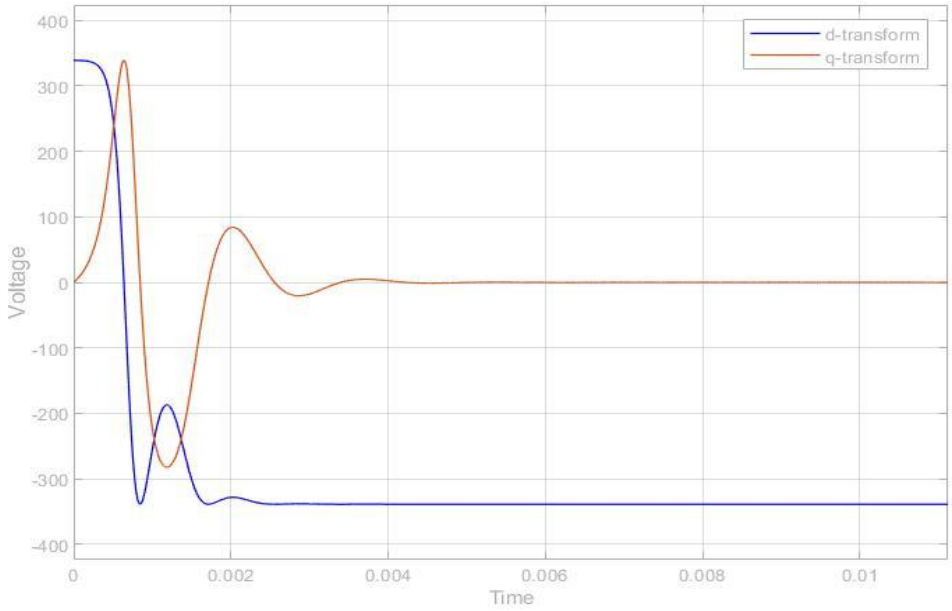

Figure 3.4: dq0 transform of Grid V_{abc}

3.2 Control Scheme

The control scheme for three phase operation consists of two parts. First is the PWM generation for gate control of AC-DC converter and second is for PWM generation for gate control of DC-DC buck boost converter. To synchronize the photovoltaic system output and the AC grid a PLL (phase-locked loop) was implemented, carrying out the angle detection in the grid. PID controllers are used for error detection and correction and the final signal is fed to the PWM generator.

Three-phase V_{abc} is converted to dq0 parameters. The abc to dq0 block uses the Park conversion to convert a three-phase (abc) signal into a rotating reference frame for dq0. The angular area of the rotating frame is given input ωt. This allows for easy control of the section. The dq0 to abc block uses the opposite Park modification to convert the dq0 rotating reference frame into a three-phase (abc) signal. The angular position of the rotating frame is given to the input ωt, on the rad. When the orientation of the rotating frame ωt = 0 is 90 degrees after the phase A axis, successive signal with Mag = 1 and Category = 0 degrees produces the following dq values: d = 1, q = 0. [19]

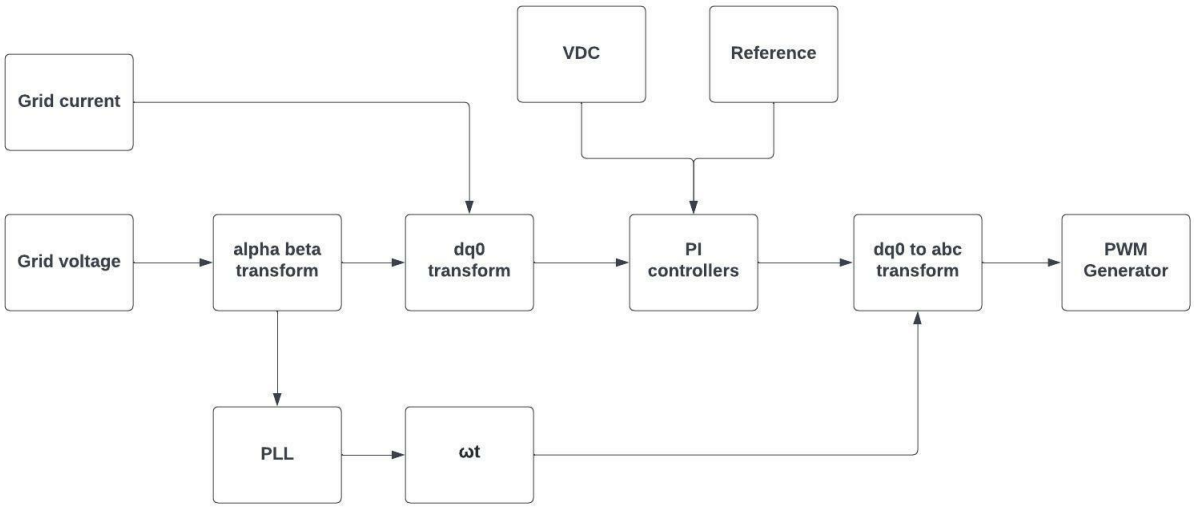

Figure 3.5: Control scheme overview for 3-phase AC-DC converter

V_{abc} is transformed into alpha beta using Clark transforms and into dq0 using Park transforms. Alphabeta transform is used to calculate ωt using PLL.

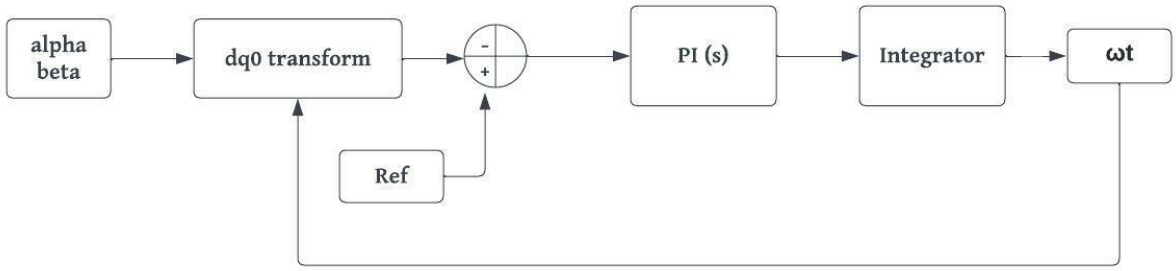

Figure 3.6: Phase locked loop overview

V_{abc} and I_{RYB} are transformed into dq0 using Park transforms into V_D , V_Q and I_D , I_Q respectively. AC-DC converter control has two parts, voltage control and current control. Both of them take dq0 transformed inputs which are later combined and transformed into abc form using the angle from PLL to maintain synchronization.

3.2.1 Voltage control for AC-DC converter

For voltage control for AC-DC 3-phase converter:

$$e(t) = (V_{dc} - V_{ref}) \tag{3.1}$$

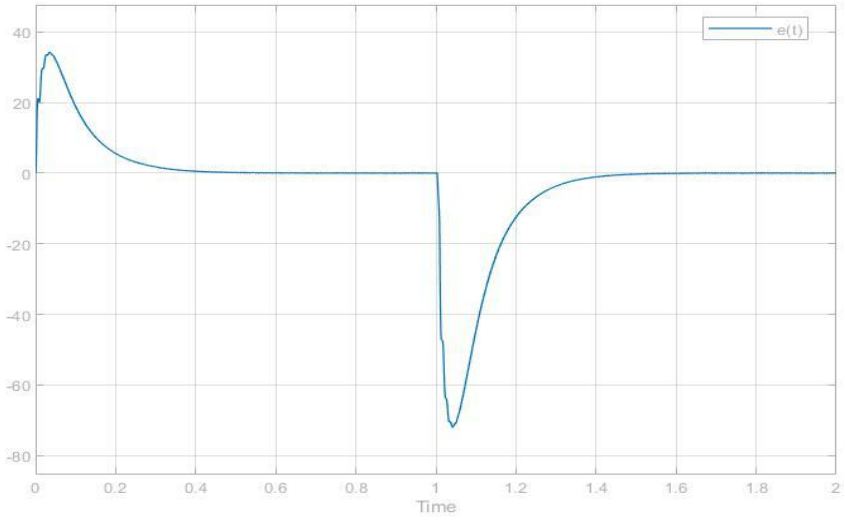

Figure 3.7: *e(t)* plot

$$r(t) = [K_p e(t) + K_i \int e(t)dt] + I_D \quad (3.2)$$

$$r(t) = [0.5e(t) + 5\int e(t)dt] + I_D \quad (3.3)$$

$$A(t) = [K_p r(t) + K_i \int r(t)dt] + 2\pi f I_Q + V_D \quad (3.4)$$

$$A(t) = [25r(t) + 500\int r(t)dt] + 2 * 10^{-3}\pi I_Q + V_D \quad (3.5)$$

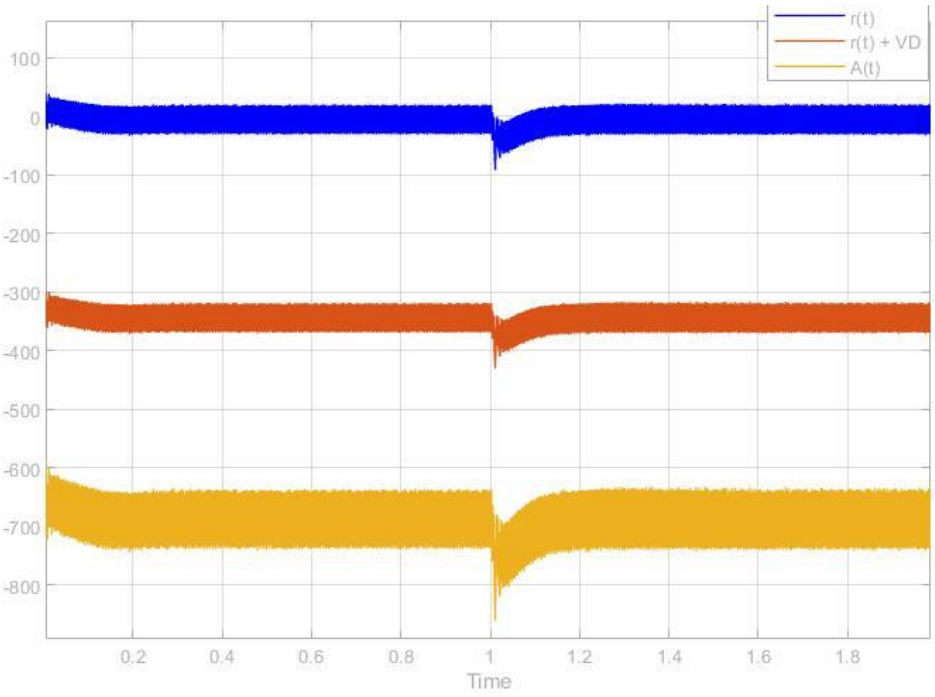

Figure 3.8: *r(t)* and *A(t)* plot

$$U(t) = \frac{2A(t)}{V_{DC}} \quad (3.6)$$

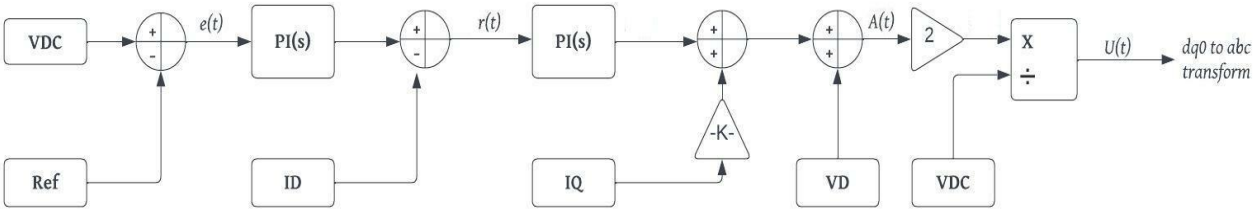

Figure 3.9: Voltage control for AC-DC 3-phase converter

3.2.2 Current control for AC-DC converter

For current control for AC-DC 3-phase converter:

$$s(t) = (I_Q - I_{ref}) \tag{3.7}$$

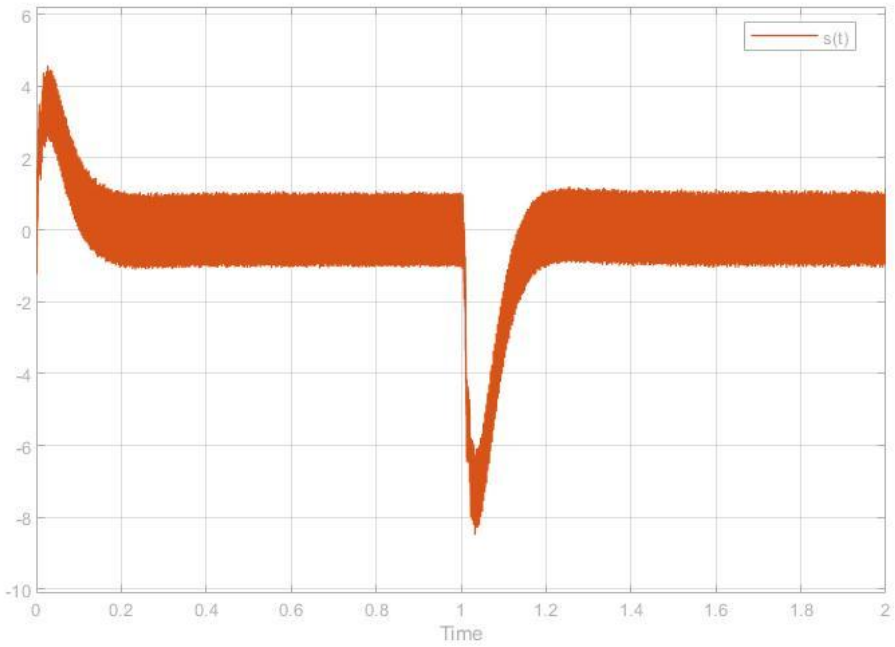

Figure 3.10: *s(t)* plot

$$C(t) = [K_p s(t) + K_i \int s(t)dt] + 2\pi f I_D + V_Q \tag{3.4}$$

$$C(t) = [25s(t) + 500 \int r(t)dt] + 2 * 10^{-3} \pi I_D + V_Q \tag{3.5}$$

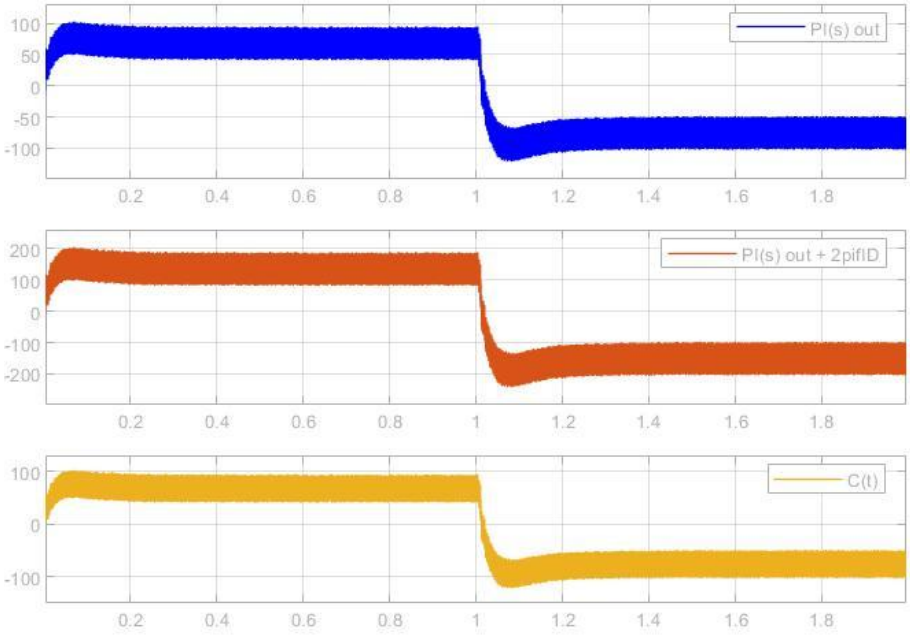

Figure 3.11: *C(t)* output plot

$$V(t) = \frac{2C(t)}{V_{DC}} \tag{3.6}$$

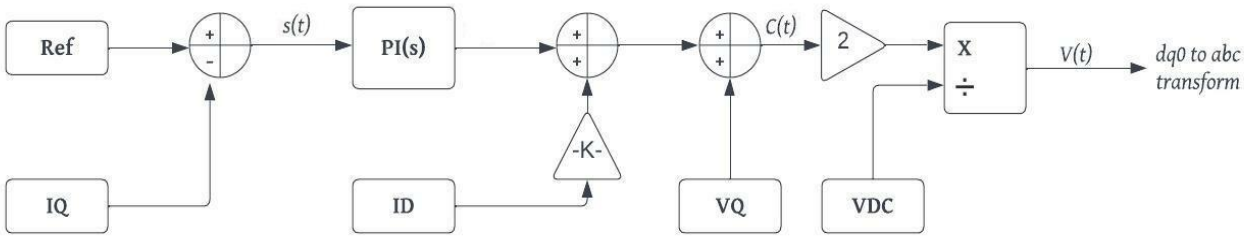

Figure 3.12: Current control for AC-DC 3-phase converter

Control for the DC-DC converter is the same single phase operation. Following is the complete control diagram for DC-DC buck boost converter:

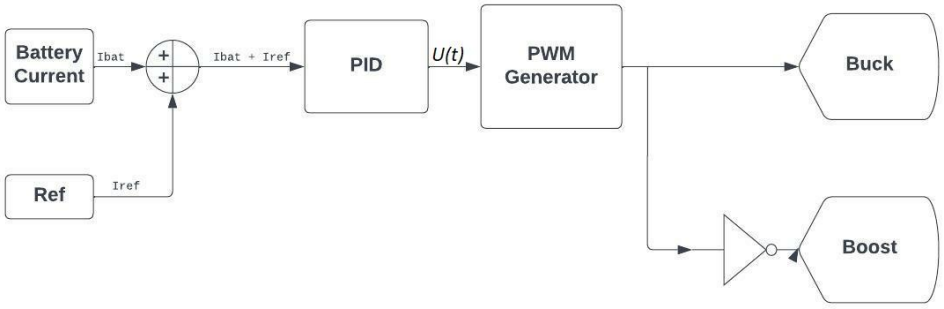

Figure 3.13: Control diagram for DC-DC Buck Boost converter

3.3 Simulation

The MATLAB simulation of three phase bi-directional operation is as follows:

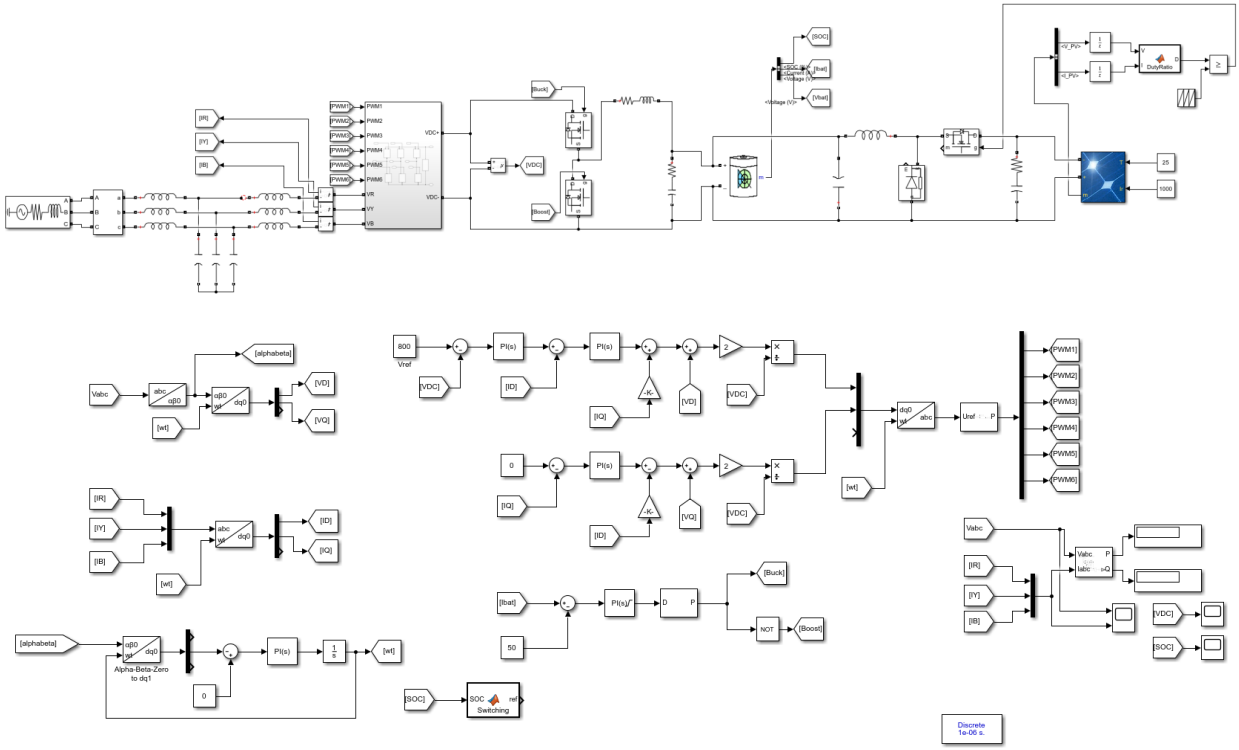

Figure 3.14: Three-Phase V2G and G2V MATLAB Simulation

Three phase grid is represented by a 415V 3-phase AC source. EV is represented by a 360V Lithium-ion battery. The system starts in G2V mode and switches over to V2G mode after 1s.

The power transfer can be observed from the active and reactive power plot of the grid. Active power is negative for G2V mode and becomes positive during V2G mode.

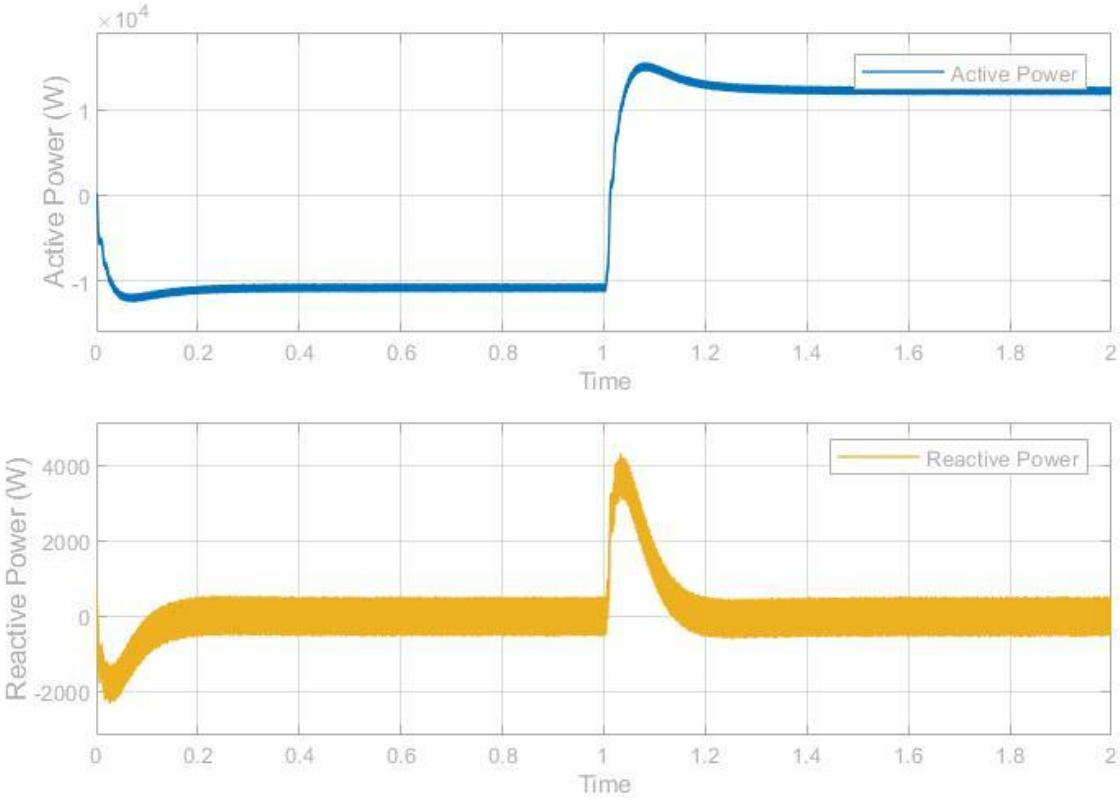

Figure 3.15: Power plot of 3-phase grid

State of charge (SOC) of the EV battery changes with the operation mode of the system. It increases in G2V mode and decreases in V2G mode.

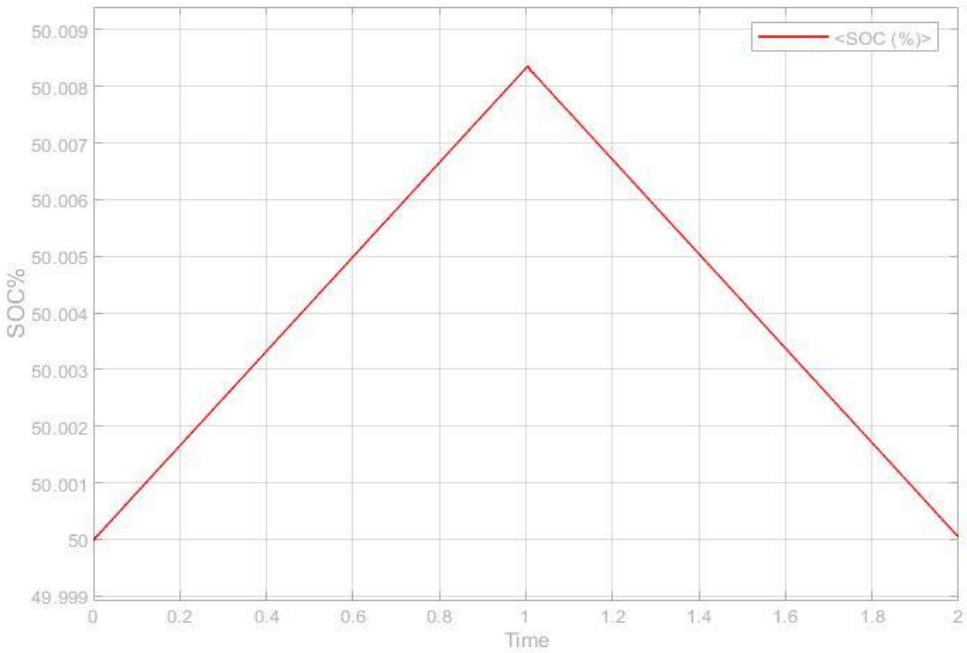

Figure 3.16: SOC(%) of the EV battery in 3-phase operation

The voltage across the DC link (VDC) returns back to reference voltage at steady state during 3-phase system operation

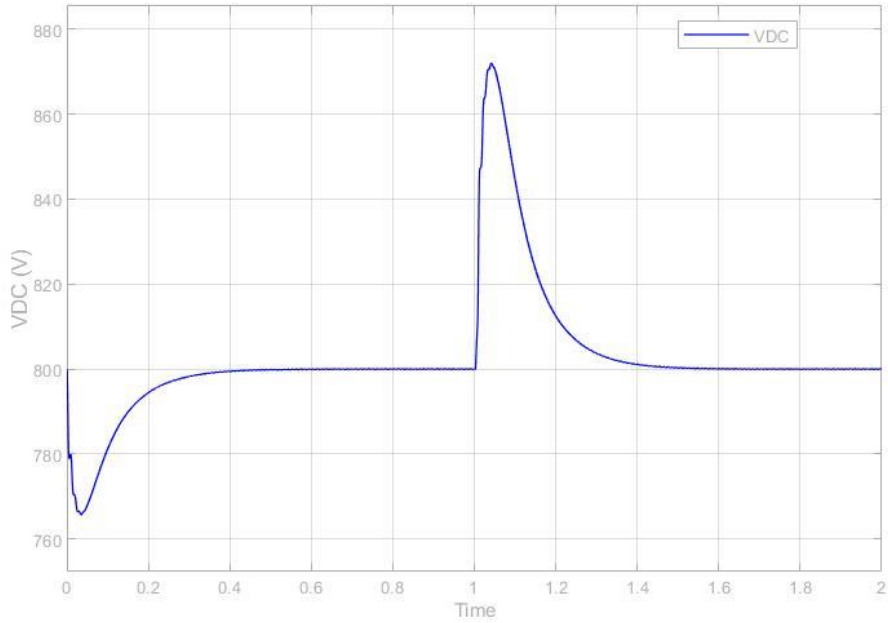

Figure 3.17: VDC plot for 3-phase operation

EV Battery voltage increases during G2V operation and battery current is negative. EV Battery voltage decreases during V2G operation and battery current is positive.

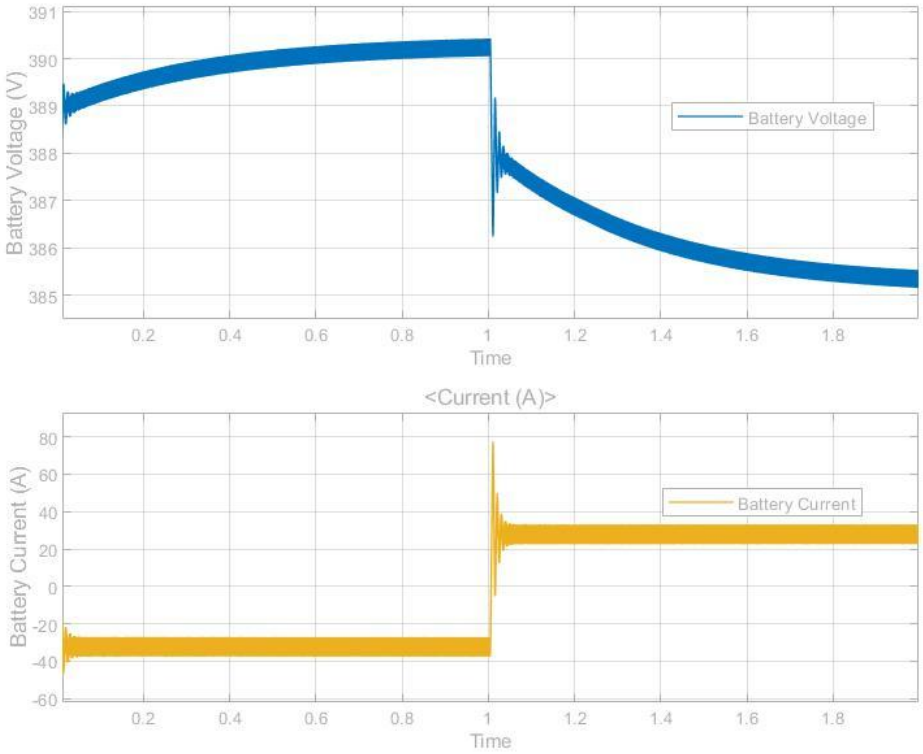

Figure 3.18: EV Battery voltage and current during 3-phase operation

3.5. Conclusion

The Bi-directional charging system is successfully demonstrated in both G2V and V2G operation for three-phase system. Charging and discharging of the battery can be observed represented by increase and decrease in battery voltage and change in the active power component of the grid. Following parameters are observed during the operation:

EV Battery steady state average current during G2V mode = - 33A
EV Battery steady state average current during V2G mode = 27 A

EV Battery steady state average voltage during G2V mode = 390.2 V
EV Battery steady state average voltage during V2V mode = 385.3 V

Steady state VDC voltage ripple = 0.3V

% SOC increase after 1s of operation in G2V mode = 0.0082%

Average active power in steady during G2V mode = -1.21×10^4 W
Average active power in steady during V2G mode = 1.34×10^4 W

Chapter 4
Improving system performance with ANN

The system was designed to have constant irradiance and temperature values for the PV module. Introducing real world values to the system causes system instability which can be observed in increase in ripples in VDC and increase in time required to achieve steady state. This could be addressed by fine tuning the PID controllers to some extent but due to the unpredictable nature of the sun and various other environmental factors, it is very difficult to tune the controller for every single outcome.

In order to expand the robustness and adaptive capabilities of the system, Artificial Neural Networks (ANNs) are employed [11]. Artificial neural networks (ANNs) use learning algorithms that can independently make adjustments as they receive new input [12]. This makes them a very effective tool for non-linear statistical data modeling.

4.1. Artificial Neural Network (ANN)

Artificial Neural Networks (ANN) are derived from the structure of the brain. Similar to the brain that has neurons interconnected to each other to relay information, artificial neural networks also have neurons that interconnect each other and relay information[25].

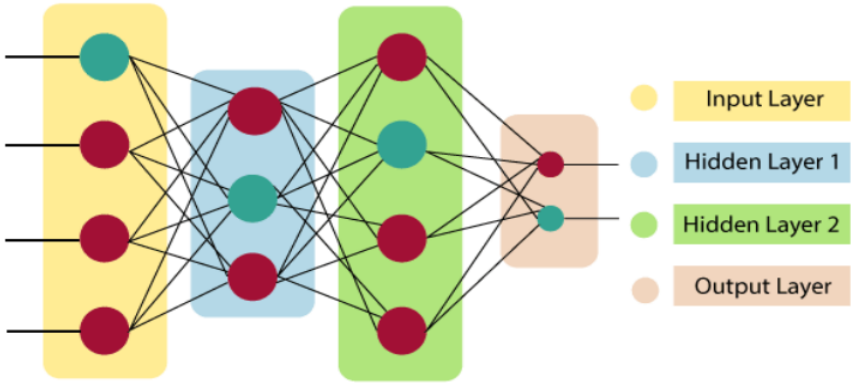

Figure 4.1: Artificial Neural Network overview

Artificial Neural Network primarily consists three types of layers:

Input Layer: It accepts the data as input and number of neurons it has is based around the number of inputs.

Hidden Layer: Hidden layer performs all the necessary calculations and operations. Number of neurons are not limited and can be any value based on requirements.

Output Layer: Input goes through a series of transformations and calculations in the hidden layer to finally result in the output that is conveyed using this layer.

The Artificial Neural Network [13] can best be represented as a weighted target graph, in which artificial neurons form nodes. The connection between the output of the neuron and the input of the neuron can be regarded as the weighted directed ends. The Artificial Neural Network receives an input signal from an external source in the form of a pattern and an image in the form of a vector.

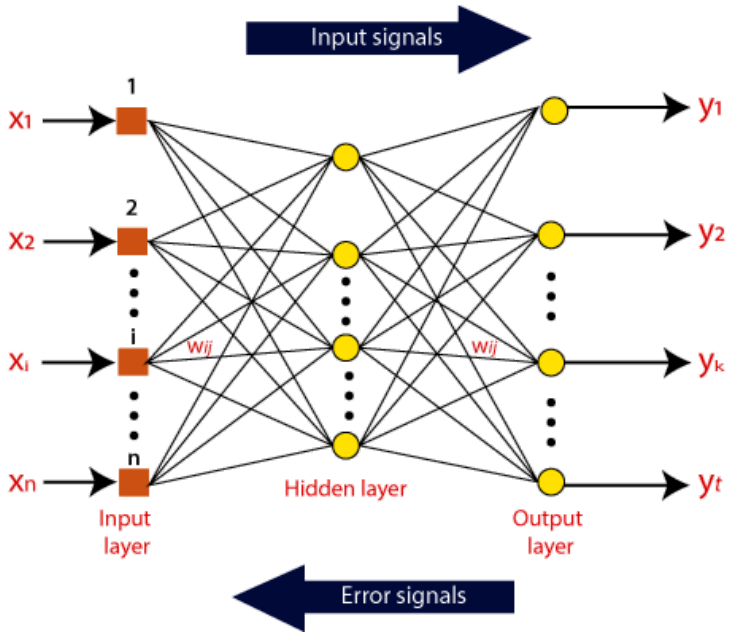

Figure 4.2: Working of weights and neurons in ANN

Each input is multiplied by its corresponding weights. In general, these weights often represent the ability to communicate between neurons within the artificial neural network. All weighted inputs are summarized within the computer unit. If the measured value is equal to zero, then bias will be added so that it is not zero. Weights can range from 0 to infinity, so to limit the value, using the activation function.

4.2. Simulation with adaptive ANN controller

Simulation is done in MATLAB Simulink software. Traditional PID controller is replaced with an adaptive ANN controller to improve the system stability [14]. The network used in the simulation is a Feed-Forward ANN which is a basic neural network consisting of an input and an output layer with at least one hidden layer.

Activation functions chosen for the layers are:

- Tan-sigmoid: For input and hidden layers
- Pure-Linear: For the output layer

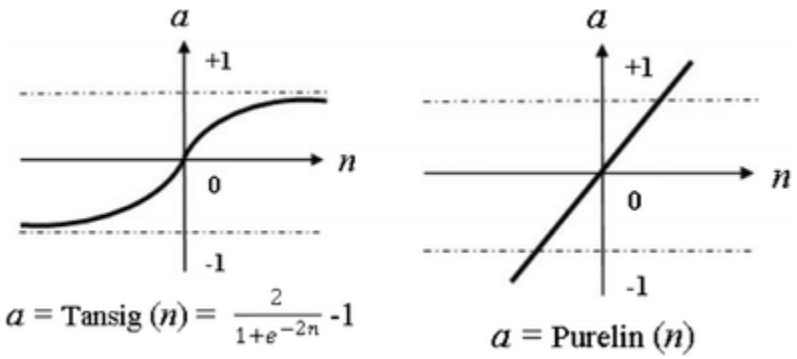

Figure 4.2: Activation functions used for ANN

Training data is given as follows:

Table 4.1: ANN Training details

Description	Parameter
ANN type	Feed forward network
Number of Hidden Layers	3
Number of Neurons for Hidden Layers	10, 20, 10
% Data used for training	70%
% Data used for testing	30%
Number of epochs	252

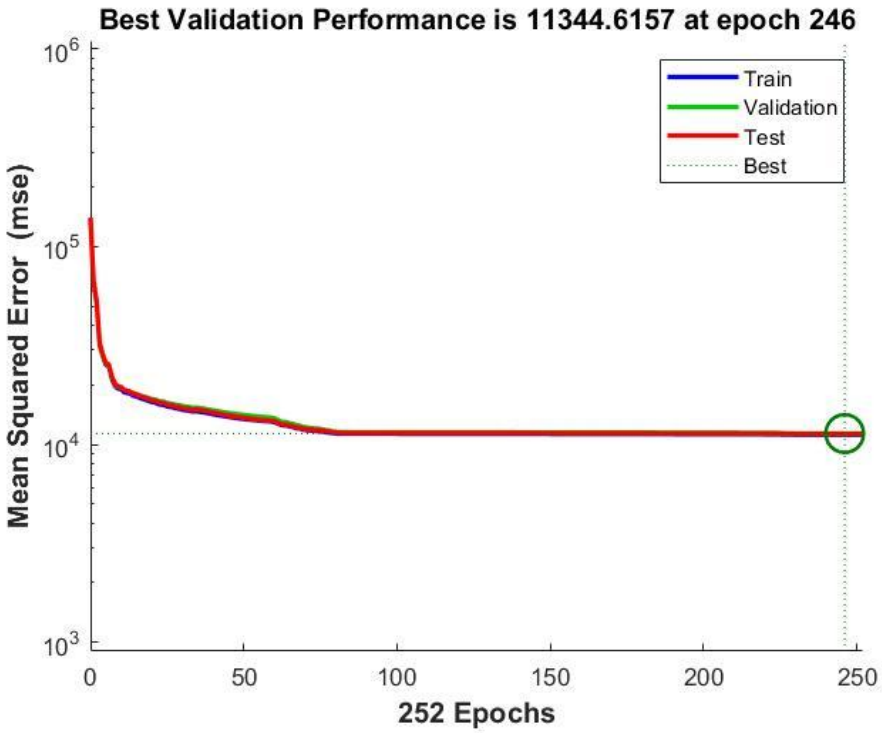

Figure 4.3: Mean squared error during training

The artificial neural network is trained with data from a single-phase bi-directional system at constant irradiance and temperature.

Simulation is a single phase bi-directional charging system similar to the previous simulation but with non-constant values for irradiance and temperature for the PV module.

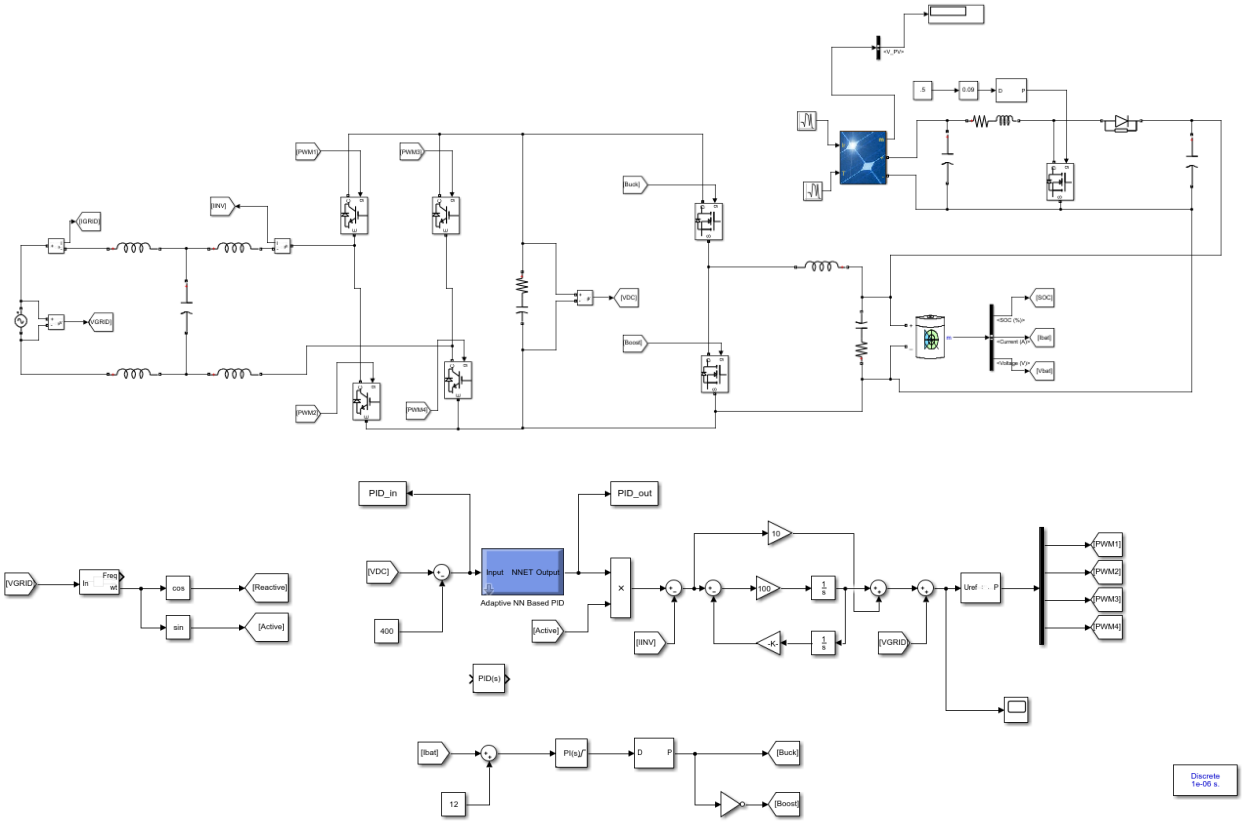

Figure 4.4: MATLAB Simulink simulation for ANN based Single-phase bi-directional charger

EV in G2V mode hence, power is transferred from the grid to the EV battery. This can be observed from the SOC plot of the battery.

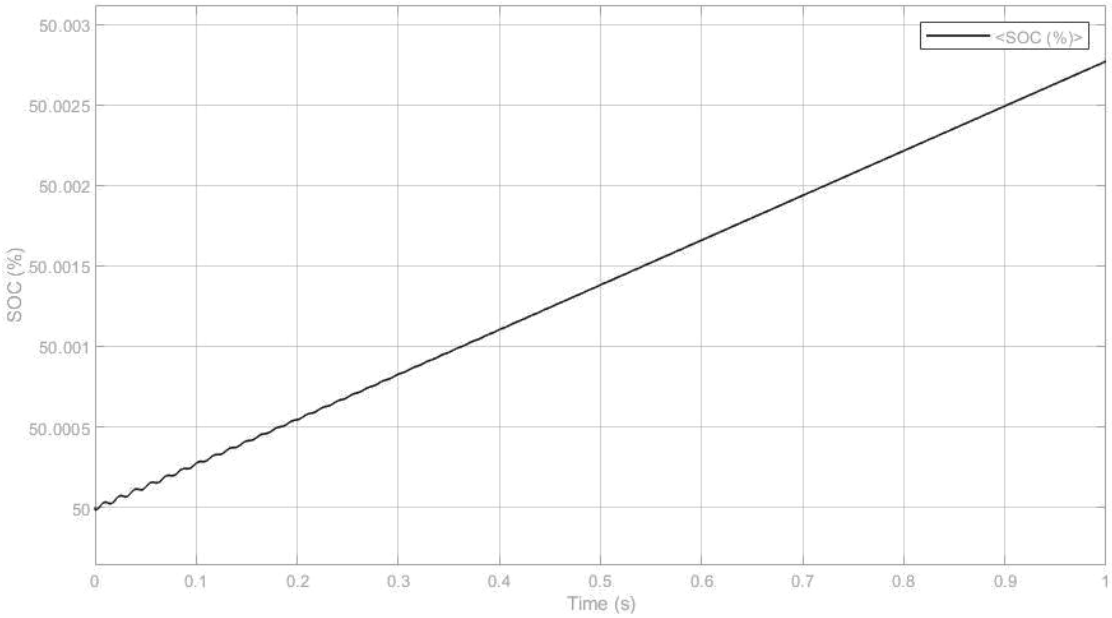

Figure 4.5: SOC level during G2V mode in ANN based system

VDC across the bi-directional converter during the charging is given by following plot:

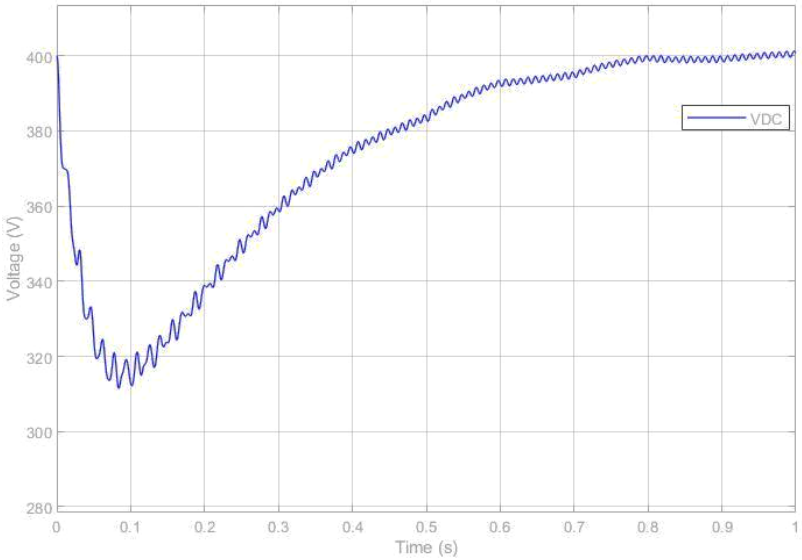

Figure 4.6: VDC across converter during G2V mode in ANN based system

4.3. Comparison against ANN based system

Following are the plots for VDC across the converter for single-phase bi-directional systems in G2V mode. Both the systems are simulated against the same conditions with non-constant values for irradiance and temperature for the PV module.

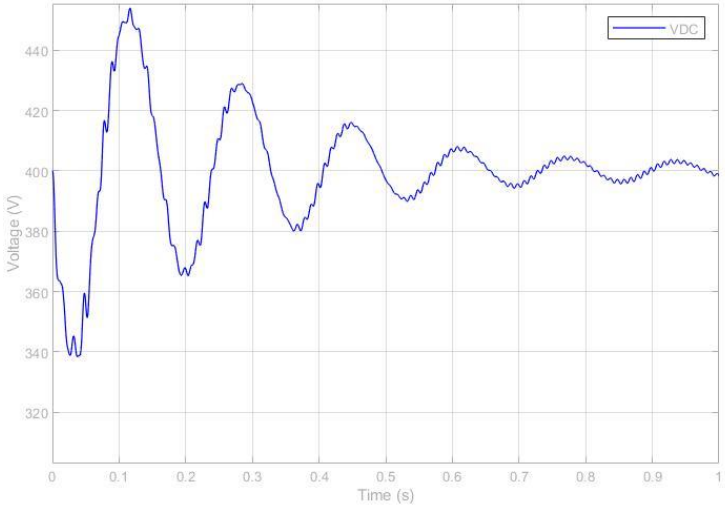

Figure 4.7: VDC across converter in system without ANN based control

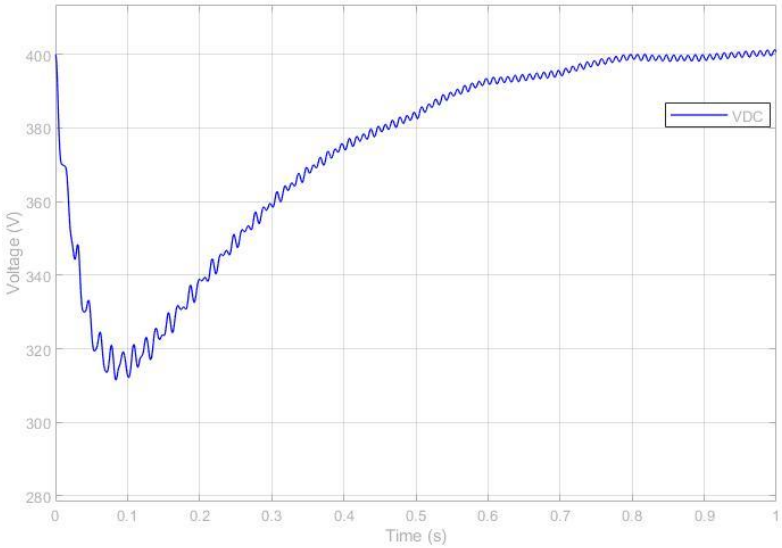

Figure 4.8: VDC across converter in system with ANN based controller

It can be observed that the system with ANN based controller achieves steady state earlier than the system without an ANN based controller. The ripple voltage is also lower in the system with an ANN based controller.

Table 4.1: Comparison between ANN and Traditional control

Description	ANN Based Control	Traditional Control
Time required to achieve steady state	0.873s	1.267s
Ripple voltage at steady state	0.72V	1.39V

From above plots and data, it is very prevalent that system stability in the system with ANN control compared to the system with traditional control.

4.4. Conclusion

Single phase bi-directional system for solar EV using Adaptive ANN controller has been designed. Adaptive ANN controller have been trained using training data set from PID controller tuned for specific conditions.

Adaptive ANN controller's performance have been compared to the traditional PID controller and following observations have been made.

Time required to achieve steady state for ANN = 0.873s
Time required to achieve steady state for traditional PID = 1.267s
Ripple voltage at steady state in ANN = 0.72V
Ripple voltage at steady state in traditional PID = 1.39V

Chapter 5
References

[1]. Kang Miao Tan, Vigna K. Ramachandaramurthy, Jia Ying Yong. Bidirectional battery charger for electric vehicles. IEEE Innovative Smart Grid Technologies - Asia (ISGT ASIA) (2014) 10.1109/ISGT-Asia.2014.6873826

[2]. Kotla Aswini , Jillidimudi Kamala , Lanka Sriram, Bhasuru Kowshik , Bugatha Ram Vara Prasad, Damaraju Venkata Sai Bharani. Design and Analysis of Bidirectional Battery Charger for Electric Vehicle. IJERT Volume 10, Issue 07 (July 2021), IJERTV10IS070226

[3]. Marco Jung, Georgios Lempidis, Joerg Kirchhof. Multifunctional bidirectional Charging of Electric Vehicles Combined wired and wireless. Conference: Symposium Hybrid- und ElektrofahrzeugeAt: Braunschweig.

[4]. M. Jung, G. Lempidis, D. Holsch, and J. Steffen, “Optimization considerations for interleaved DC-DC converters for EV battery charging applications, in terms of partial load efficiency and power density,” in 2015 17th European Conference on Power Electronics and Applications (EPE '15 ECCE Europe), pp. 1–9.

[5]. Tatsuya IZUMI*, Masayoshi Hirota, Kenichi Hatakama, Yoshikazu Isoyama, Katsuhiko Sano and Koichi Takayama. Bidirectional Charging Unit for Vehicle-to-X (V2X) Power Flow. Sei Technical Review, number 79, October 2014.

[6]. Yakup Sahin, Naim Suleyman Ting. Design of A New Bidirectional DC-DC Converter. INCES 2019 pp. 228-233. October 2019

[7]. Sairatun Nesa Soheli; Golam Sarowar; Md. Ashraful Hoque; Md Saidul Hasan. Design and Analysis of a DC -DC Buck Boost Converter to Achieve High Efficiency and Low Voltage Gain by using Buck Boost Topology into Buck Topology. ICAEEE 2018. 10.1109/ICAEEE.2018.8643001

[8]. Dong Xie; Dajin Zhang; Peng Gao. Research on phase-locked loop control and its application IEEE Information Technology, Networking, Electronic and Automation Control Conference

(2016). DOI: 10.1109/ITNEC.2016.7560475

[9]. Mboumboue, Edouard & Njomo, Donatien. (2013). Mathematical Modeling and Digital Simulation of PV Solar Panel using MATLAB Software. International Journal of Emerging Technology and Advanced Engineering. Volume 3.

[10]. Nadia, Mars & Lassad, Houcine & Zaafouri, Abderrahmen & Chaari, Abdelkader. (2020). Influence of temperature and irradiance on the different solar PV panel technologies. International Journal of Energy Sector Management. ahead-of-print. 10.1108/IJESM-06-2020-0002.

[11]. A. Mathur and T. Samad, "Neural networks-a tutorial for the power industry," Proc. Am. Conf., vol 52, pp. 239-244, 1990.

[12]. T S Dillon, "Artificial neural network applications to power systems and their relationships to symbolic methods," Electrical Power & Energy.

[13]. František Kudlačák; Tibor Krajčovič. Artificial neural network for adaptive PID controller Cybernetics & Informatics (K&I) (2018), DOI: 10.1109/CYBERI.2018.8337564

[14]. Daouda Gueye; Alphousseyni Ndiaye; Amadou Diao. Adaptive Controller Based on Neural Network Artificial to Improve Three-phase Inverter Connected to the Grid. ICERA 27-30 Sept. 2020. 10.1109/ICRERA49962.2020.9242740

[15]. Hall P J et al. 2010 Energy storage in electrochemical capacitors: designing functional materials to improve performance Energy Environ. Sci. 3 1238–51

[16]. Y. Hu, Y. Du, W. Xiao, S. Finney, W. Cao; DC-link voltage control strategy for reducing capacitance and total harmonic distortion in single-phase grid-connected photovoltaic inverters IET Power Electron, 8 (8) (2015), pp. 1386-1393

[17]. Taqi ur Rahman1, Salman Amin1 and Shaikh Saaqib Haroon; A novel methodology for volume reduction of HV capacitors using highly electronegative composite nano materials.

[18]. O'Rourke, Colm J. et al. "A Geometric Interpretation of Reference Frames and Transformations: dq0, Clarke, and Park." IEEE Transactions on Energy Conversion 34, 4 (December 2019): 2070 -2083 © 2019 IEEE.

[19] Krause, P., O. Wasynczuk, S. D. Sudhoff, and S. Pekarek. Analysis of Electric Machinery

and Drive Systems. Piscatawy, NJ: Wiley-IEEE Press, 2013.

[20] A. Shukla, K. Verma, and R. Kumar, “Impact of EV fast charging station on distribution system embedded with wind generation,” J. Eng., vol. 2019, no. 18, pp. 4692–4697, 2019 doi: 10.1049/joe.2018.9322.

[21] Bugatha Ram Vara prasad T.deepthi n.satyavathi v.satish varma r.hema kumar, “Solar charging station for electric vehicles,” Int.J. Adv. Res. Sci. Commun. Technol., vol. 7, no. 2, pp. 316–325,2021, doi: 10.48175/IJARSCT-1752.

[23] BUGATHA RAM VARA PRASAD, C. PRASANTHI, G.JYOTHIKA SANTHOSHINI, K. J. S. V. KRANTI KUMAR,and K. YERNAIDU, “Smart Electrical Vehicle,” i-manager’s J.Digit. Signal Process., vol. 8, no. 1, p. 7, 2020, doi:10.26634/jdp.8.1.17347.

[24] Atul R. Saraf and M. Sadaiah, “Application of artificial intelligence for the prediction of undercut”, International Journal of Mechatronics and Mechatronics Systems, Vol.6 (2), pp.183-194, 2013.

[25] G. Krishna Mohana Rao and G. Rangajanardhaa, “Development of hybrid model and optimization of surface roughness in electric discharge machining using artificial neural networks and genetic algorithm”,

[26] Malik, Monu & Dahiya, Ratna. (2020). Optimization of DC-DC Converters for Off-Grid Lighting in Trains Using Artificial Neural Networks. 10.1007/978-981-13-8618-3_36.

[27] Masri, Syafrudin & Mohamad, Norizah & Hafeez, Muhammad. (2012). Design and development of DC-DC buck converter for photovoltaic application. 2012 International Conference on Power Engineering and Renewable Energy, ICPERE 2012. 1-5. 10.1109/ICPERE.2012.6287236.

[28] Rashid, M.. (2022). Power electronics : circuits, devices, and applications / Muhammad Harunur Rashid. SERBIULA (sistema Librum 2.0).

[29] Meksarik, V. & Masri, Syafrudin & Taib, Soib & Hadzer, Che. (2004). Development of high efficiency boost converter for photovoltaic application. 153 - 157. 10.1109/PECON.2004.1461634.